CHEMISTRY
A EUROPEAN JOURNAL

FULL PAPER

DOI: 10.1002/chem.201200279

sp^2-Iminosugar *O*-, *S*-, and *N*-Glycosides as Conformational Mimics of α-Linked Disaccharides; Implications for Glycosidase Inhibition

Elena M. Sánchez-Fernández,[a] Rocío Rísquez-Cuadro,[b] Carmen Ortiz Mellet,*[b] José M. García Fernández,[a] Pedro M. Nieto,[a] and Jesús Angulo*[a]

Abstract: The synthesis of mimics of the α(1→6)- and α(1→4)-linked disaccharides isomaltose and maltose featuring a bicyclic sp^2-iminosugar nonreducing moiety *O*-, *S*-, or *N*-linked to a glucopyranoside residue is reported. The strong generalized anomeric effect operating in sp^2-iminosugars determines the α-stereochemical outcome of the glycosylation reactions, independent of the presence or not of participating protecting groups and of the nature of the heteroatom. It also imparts chemical stability to the resulting aminoacetal, aminothioacetal, or *gem*-diamine functionalities. All the three isomaltose mimics behave as potent and very selective inhibitors of isomaltase and maltase, two α-glucosidases that bind the parent disaccharides either as substrate or inhibitor. In contrast, large differences in the inhibitory properties were observed among the maltose mimics, with the *O*-linked derivative being a more potent inhibitor than the *N*-linked analogue; the *S*-linked pseudodisaccharide did not inhibit either of the two target enzymes. A comparative conformational analysis based on NMR and molecular modelling revealed remarkable differences in the flexibility about the glycosidic linkage as a function of the nature of the linking atom in this series. Thus, the *N*-pseudodisaccharide is more rigid than the *O*-linked derivative, which exhibits conformational properties very similar to those of the natural maltose. The analogous pseudothiomaltoside is much more flexible than the *N*- or *O*-linked derivatives, and can access a broader area of the conformational space, which probably implies a strong entropic penalty upon binding to the enzymes. Together, the present results illustrate the importance of taking conformational aspects into consideration in the design of functional oligosaccharide mimetics.

Keywords: carbohydrates · conformation analysis · inhibitors · molecular modeling · structural biology

Introduction

Glycosidases, enzymes that catalyze the cleavage of glycosidic bonds in oligosaccharides and glycoconjugates, are fundamental to a broad range of biological processes including the degradation of dietary polysaccharides, the lysosomal catabolism of glycoconjugates, and the biosynthesis of the oligosaccharide units in glycoproteins and glycolipids, which in their turn are involved in a plethora of cell communication events. Consequently, inhibitors of these enzymes possess strong therapeutic potential for the treatment of ailments as varied as diabetes,[1] lysosomal storage disorders,[2] viral infection,[3] and cancer.[4] Critical to these channels is the development of compounds that can discriminate between glycosidases acting on different substrates, in different tissues or in different cell compartments. For instance, the lack of sufficient anomeric selectivity towards α- or β-glucosidases is largely responsible for the failure of classical iminosugar-type inhibitors, such as 1-deoxynojirimycin (**1**) or castanospermine (**2**), in clinical trials (Figure 1).[5]

In principle, one could expect that higher selectivities within isoenzyme series could be achieved by mimicking not

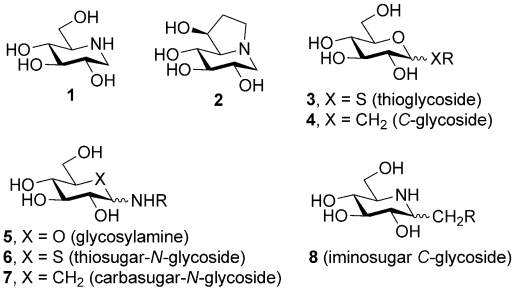

Figure 1. Structures of glycomimetic representatives either without (**1** or **2**) or with (**3**–**8**) pseudoaglycone substituents.

[a] Dr. E. M. Sánchez-Fernández, Prof. J. M. García Fernández, Dr. P. M. Nieto, Dr. J. Angulo
Instituto de Investigaciones Químicas (IIQ)
CSIC–Universidad de Sevilla
Avda. Americo Vespucio 49
41092, Sevilla (Spain)
Fax: (+34) 954460565
E-mail: jesus@iiq.csic.es

[b] R. Rísquez-Cuadro, Prof. C. Ortiz Mellet
Departmento de Química Orgánica
Facultad de Química
Universidad de Sevilla
C/Prof. García González 1
41012, Sevilla (Spain)
Fax: (+34) 954624960
E-mail: mellet@us.es

Supporting information for this article is available on the WWW under http://dx.doi.org/10.1002/chem.201200279.

only the glycone but also the anomeric stereochemistry and the aglycone portion of the natural substrate.[6] If properly arranged, once the glycone moiety is accommodated in the catalytic (−1) site of the enzyme, an anomeric substituent may bind to the adjacent aglycone (+1) subsite, which, depending on the enzyme, can be adapted to the binding of sugar, acyl group, or other types of moieties. The choice of linkage type to span the glycone and aglycone binding sites is not trivial. Replacing the glycosidic oxygen in natural glycosides by other atoms, such as sulfur (**3**) or carbon (**4**), has been shown to lead to compounds that are recognized by glycosidases, acting as moderate to good inhibitors (Figure 1).[7] Yet, differences in the conformation of these molecules with respect to the natural compounds have been reported, the origin of which has been the subject of some controversy.[8] Moreover, such chemical modifications can alter the stereoelectronic barriers for rotation about the glycosidic linkage. 3D shapes compatible with enzyme binding can then be obtained by conformational variations that do not imply chair distortion, leading to differences in the preferred bound conformations.[9] Nitrogen-linked analogues (**5**–**7**) would be particularly interesting because anomeric amino groups can provide additional interactions with the catalytic carboxylic groups,[10] but the instability and lack of configurational integrity of aminoacetal (**5**)[11] and aminothioacetal functionalities (**6**)[12] limits this approach to carbasugar-type (**7**)[13] or nonglycosidically-linked glycomimetics.[14] The use of iminosugar-type glycone moieties faces similar instability problems for the elaboration of *O*- or *S*-glycosides and is only compatible with the *C*-glycoside prototype (**8**),[15] which implies a relatively complex chemistry and sacrifices the contribution of the *exo*-anomeric effect to the conformational equilibrium (Figure 1).[16]

In previous work, we showed that replacing the sp^3-amine nitrogen typical of iminosugars by a pseudoamide-type nitrogen, with substantial sp^2-character (sp^2-iminosugars), results in inhibitors for which the α- or β-glycosidase anomeric selectivity can be modulated through nonglycone interactions upon the installation of appropriate substituents at specific locations.[17,18] Interestingly, 1-deoxy-2-oxa-3-oxocastanospermine derivatives with alkyl *O*-, *S*-, or *N*-pseudoanomeric groups (**9**) acted as specific inhibitors of neutral α-glucosidases, exhibiting antiproliferative activity against human breast carcinoma cells in vitro.[19] In those compounds, the glycone specificity is presumed to be conferred by the structural similarity of the polyhydroxylated core with D-glucopyranose. The very intense anomeric effect in sp^2-iminosugars, which is ascribable to a very efficient overlap between the π-symmetrical orbital located on the lone-pair of the endocyclic nitrogen and the σ* antibonding orbital of the anomeric C–X bond, imparts chemical, conformational and configurational stability to the axially oriented pseudoaglycone substituent, and is probably responsible for the remarkable α-selectivity (Figure 2).[20] The bicyclic piperidine-carbamate core appears then to be an ideal scaffold for the design of linkage-spanning α-glucosidase inhibitors in which the glycone and aglycone portions can be brought together

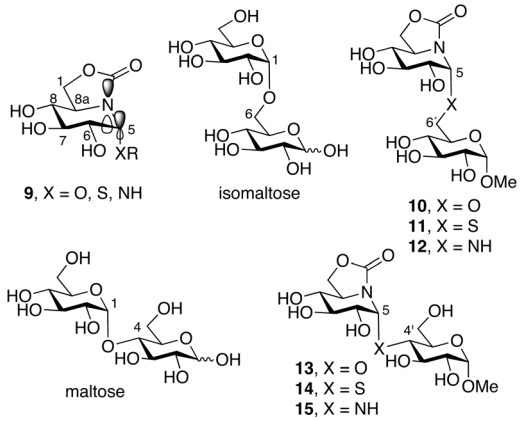

Figure 2. General structure of bicyclic carbamate-type sp^2-iminosugars showing the key orbitals involved in the anomeric effect (**9**) and structures of the isomaltose (**10**–**12**) and maltose mimics (**13**–**15**) prepared in this work. The numbering of the sp^2-iminosugar moiety follows the numbering system used for the indolizidine system (e.g., as for castanospermine **2**).

through oxygen, sulfur, or nitrogen heteroatoms. This offers a unique opportunity to conduct a systematic study on the consequences of differences in the conformational behavior within homologous series of compounds in their enzyme inhibitory properties, which would be of great relevance for the proper design of second generation molecules with better properties. To test this hypothesis, we have focused on two closely related α-glucosidases from *S. cerevisae*, oligo-α-1,6-glucosidase (EC 3.2.1.10, isomaltase) and α-1,4-glucosidase (EC 3.2.1.20, maltase). Both enzymes belong to family GH 13 in the CAZy classification.[21] Maltase preferentially hydrolyses maltose, but not isomaltose (which acts act as competitive inhibitor),[22] whereas isomaltase hydrolyzes isomaltose but not maltose (which acts as a competitive inhibitor).[23] In a preliminary report, we noted that the *gem*-diamine-type isomaltose and maltose mimics **12** and **15** were actually stable compounds with the ability to bind isomaltase.[24] Herein, we compare our previous results with those for the corresponding *O*-linked (**10**, **13**) and *S*-linked disaccharide mimics (**11** and **14**, respectively) and analyse their inhibitory properties towards isomaltase and maltase (Figure 2). We show that the capabilities of binding to each enzyme are indeed strongly dependent on the chemical nature of the compound and can be correlated to differences in their conformational behavior in solution.

Results and Discussion

Synthesis: Tri-*O*-acetyl-protected derivatives of the 2-oxa-3-oxo-castanospermine skeleton represented by the general formula **9** (Figure 2) but bearing a 5-*O*-trichloroacetimidate ($X=O$; $R=C(=N)CCl_3$)[25] or a 5-bromo group ($XR=Br$) were initially considered as suitable sp^2-iminosugar pseudoglycosyl donors for the construction of the isomaltoside and maltoside mimics **10** and **13**. However, reactions with the

corresponding glycosyl acceptors using a variety of glycosylation promoters and conditions did not proceed to completion, resulting in extensive formation of the product of hydrolysis (**9**; XR = OH) after conventional work up. Alternatively, use of the corresponding pseudoglycosyl fluoride analogue **17** as precursor was attempted (Scheme 1). Compound

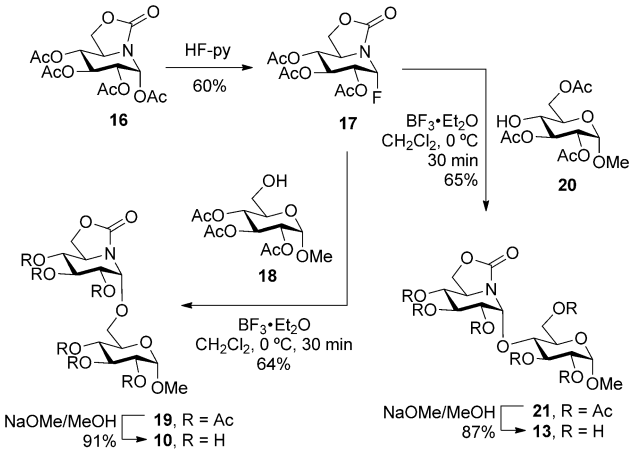

Scheme 1. Synthesis of the *O*-linked isomaltoside and maltoside mimics **10** and **13**.

17 was obtained in 60% yield as a stable solid by reaction of tetracaetate **16** with pyridinium poly(hydrogen fluoride).[26] In the presence of boron trifluoride-diethyl ether complex ($BF_3{\cdot}Et_2O$), **16** smoothly reacted with methyl 2,3,4-tri-*O*-acetyl-α-D-glucopyranoside[27] (**18**) or methyl 2,3,6-tri-*O*-acetyl-α-D-glucopyranoside[28] (**20**) in dichloromethane at 0°C to give the corresponding per-*O*-acetylated α-(5→6′) and α-(5→4′) pseudodisaccharides **19** and **21** in 64 and 65% yield, respectively. Final deacetylation under standard sodium methoxide-catalyzed conditions provided the required fully unprotected compounds **10** and **13** (Scheme 1).

sp^2-Iminosugar thioglycoside derivatives have previously been obtained from tetraacetate **16** by reaction with thiols in the presence of $BF_3{\cdot}Et_2O$.[24] However, in the case of the 6- and 4-thiousugars **22**[29] and **24**,[30] this procedure proved unsuccessful. The pseudo-*S*-disaccharides **23** and **25** could be obtained in satisfactory yield by using, instead, fluorocompound **17** as donor (Scheme 2). Minor proportions of monodeacetylated products, probably arising from sulfur-assisted regioselective deacetylation at position O-6, were detected in the crude reaction mixtures by mass spectrometry and ^1H NMR analyses. Reacetylation, column chromatographic purification, and conventional base-catalyzed removal of the ester protecting groups, afforded the target fully unprotected thioodisaccharide mimics **11** and **14** (Scheme 2).

The pseudo glucosyl fluoride **17** proved ineffective as an sp^2-iminosugar donor for the preparation of *N*-linked isomaltoside or maltoside analogues. Reaction of the unprotected bicyclic carbamate **26** with ammonia or amines in methanol has been previously shown to afford the corresponding pseudoglycosylamines.[19,24] However, Amadori re-

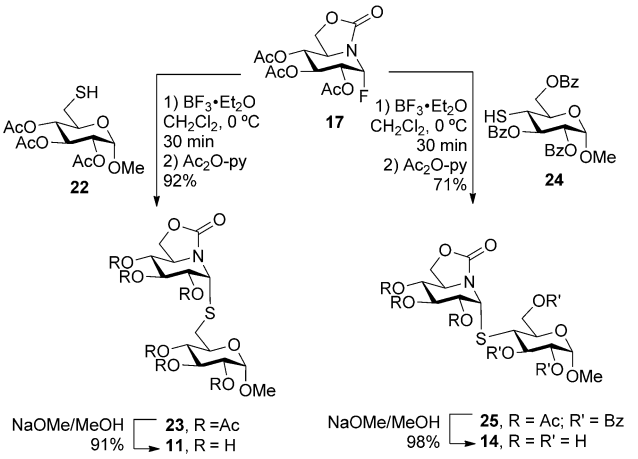

Scheme 2. Synthesis of the *S*-linked isomaltoside and maltoside mimics **11** and **14**.

arrangement[31] to give D-fructose derivatives was observed in some cases, which was found to be favored for *vic*-hydroxylamines due to their ability to undergo concomitant oxidation-intramolecular glycosylation.[24] To limit this side-reaction, coupling of **26** with methyl 6- and 4-aminodeoxy-α-D-glucopyranosides (**27**[32] and **28**[33]) in methanol was conducted under a nitrogen atmosphere (Scheme 3). The α-*N*-

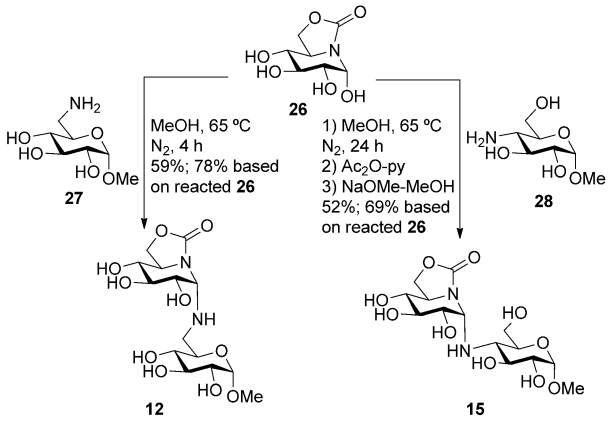

Scheme 3. Synthesis of the *N*-linked isomaltoside and maltoside mimics **12** and **15**.

(5→6′)-linked pseudoisomaltoside **12** was thus obtained in 59%, with 25% unreacted **26** recovered. In the case of the α *N*-(5→4′) maltoside mimic **15**, purification required acetylation of the reaction mixture prior to column chromatography and final deacetylation (Scheme 3).

The α-stereochemical outcome of the above reactions, confirmed by the proton-proton coupling constant values about the piperidine ring (see Experimental section) is remarkable. Glycosidation and thioglycosidation of glycosyl donors bearing participating groups at C-2 (C-6 in the indolizidine numbering system for **17**) are expected to proceed with anchimeric assistance to give preferentially the diaste-

reomer with a 1,2-*trans* relative disposition, that is, the β-anomer for D-glucopyranosyl donors.[7a] In the case of the sp^2-iminosugar **17**, however, departure of the leaving fluoro group is probably assisted by the lone-pair of the carbamate nitrogen to give a transient azacarbenium cation species (**29**; Scheme 4). Although this intermediate might be in equilibri-

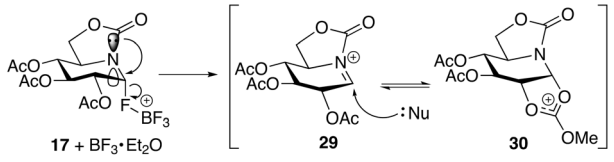

Scheme 4. Generalized anomeric effect controlled (thio)glycosidation of **17**.

um with the tricyclic orthoester oxocarbenium involving the vicinal acetoxy group (**30**), subsequent addition of the alcohol or thiol nucleophile is under strict control of the anomeric effect, affording the α-linked pseudo(thio)-disaccharide as the only reaction product (Scheme 4). The result is even more extraordinary in the case of the *N*-linked pseudodisaccharides. *gem*-Diamines typically suffer from instability under physiologically conditions[34] and the preparation of α-configured glycosylamines is particularly problematic due to the overwhelming thermodynamic preference for the β-anomer as determined by the reverse anomeric effect.[35] Together, these results strongly support the prevalence of the anomeric effect as the main driving force in reactions involving the pseudoanomeric center in sp^2-iminosugars.

Glycosidase inhibitory activity evaluation: Compounds **10**–**12** and **13**–**15** represent examples of pseudodisaccharides with a hydroxylation profile and substitution pattern of stereochemical complementarity with isomaltose and maltose, respectively, differing exclusively in the nature of the interglycosidic heteroatom. They can, in principle, mimic not only the developing glucopyranosyl cation in the reaction coordinate of enzymatic hydrolysis of α-glucosidases at the glycone (−1) site but also the aglycone moiety at the corresponding aglycone (+1) site in the cases of maltase and isomaltase, both enzymes being able to bind to either of the parent disaccharides. Actually, the three isomaltose analogues behaved as very selective inhibitors of isomaltase and maltase. No inhibition of β-glucosidases or enzymes acting on other sugar configurations was observed, and only the *N*-linked derivative exhibited a weak inhibition constant against trehalase, an enzyme acting on the α,α′(1→1)-linked disaccharide α,α′-trehalose. In all cases, the inhibitory potency against maltase was higher than against isomaltase, but no strong differences between the *O*-, *S*-, and *N*-linked derivatives were noted. The scenario totally changed in the case of α(1→4)-linked derivatives. Whereas *O*-linked pseudomaltoside was a potent and totally selective inhibitor of isomaltase and maltase, the *N*-linked analogue was a much poorer inhibitor and the S-linked derivative did not inhibit either of the two enzymes at concentrations up to 2 mM.

To ascertain whether the observed differences in the inhibitory properties could be correlated to differences in the conformational behavior of the different pseudodisaccharides, an NMR and computational analysis was conducted.

NMR studies: The conformation of the piperidine ring of the sp^2-iminosugar moiety in compounds **10**–**15** is fixed in the $^8C_5$ chair, whereas the pyranose ring in the substituted glucopyranoside moiety adopts the equivalent $^4C_1$ conformation, as inferred from the analysis of the corresponding experimental vicinal proton-proton coupling constants. Therefore, the global geometry of these pseudodisaccharides is fundamentally defined by the corresponding dihedral angles about their pseudoglycosidic linkages, that is, α(5→6′) for **10**–**12** and α(5→4′) for **13**–**15**. Due to their similarities to typical saccharide structures, we adopt the nomenclature generally used for the equivalent angles in glycosides,[36] namely ϕ (H5-C5-X-Y′; where X = O, N, or S and Y′ = C4' or C6′) and ψ (C5-X-Y′-Z′; where Z′ = H4′ or C5′). For the isomaltoside mimics **10**–**12**, the global geometry is characterized not only by the values of the ϕ and ψ torsion angles, but also by the rotamers around the C5′−C6′ bond, defined by the ω dihedral angle O6′-C6′-C5′-O5′.

By analogy with the parent disaccharides, three preferred regions on the ϕ–ψ potential energy surfaces of these compounds would be expected, namely *syn*ϕ–*syn*ψ, *syn*ϕ–*anti*ψ, and *anti*ϕ–*syn*ψ, the latter being less likely to be populated in solution due to the *exo*-anomeric effect. Concerning the ω dihedral angle, three canonical dispositions, corresponding to the staggered conformations gt, gg, and tg, must be considered. These regions could be unequivocally characterized experimentally by the detection of exclusive NOE correlations.

In the case of the *N*-linked isomaltoside mimic **12**, the pK_a of the intersaccharide amino group was found to be around 12 from a ^{1}H NMR pH titration experiment, indicating that at neutral pH this group is fully protonated and, therefore, positively charged (see the Supporting Information). This high basicity is probably a consequence of the strong contribution of orbital interactions to the anomeric effect, which implies an increase of electron density at the glycosidic bond. To determine the populations of conformers around the ω torsion angle, the vicinal J(5′,6′) coupling constants were analyzed, giving values of 2.8 Hz for H6′(*proS*) and 7.8 Hz for H6′(*proR*). A nonlinear least squares fitting of these experimental values with those theoretically predicted for the three canonical conformers gt, gg, and tg led to a distribution of populations of 80% gt and 20% gg, with no participation of the tg rotamer. The observed NOE contacts involving the methylene protons were in very good agreement with the populations determined from the coupling constant values. Thus, H5 at the iminosugar ring showed a NOE with H6′(*proS*) that was stronger than the H5/H6′(*proR*) NOE. On the other hand, the H4′/H6′(*proR*) NOE was stronger than the H4′/H6′(*proS*) NOE. Interest-

ingly, a significant NOE cross peak between protons H5 and H5′ was observed, which reported on a substantial contribution of conformers with ψ torsion around 90°, indicating that the gt conformer must exhibit considerable flexibility around this dihedral angle, oscillating between values of 180° and 90° (Figure 3, left). It was also possible to identify

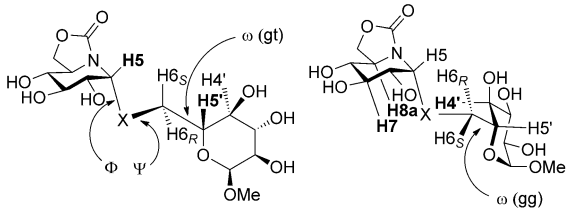

Figure 3. Schematic representation of the gt (left) and gg (right) conformations for isomaltoside mimics. Only protons involved in diagnostic NOE contacts are depicted. Exclusive NOEs for each conformation, as discussed in the text, are highlighted in bold.

a weak long-range NOE contact correlating to H8a at the sp^2-iminosugar moiety and H4′ (Figure 3, right, and Figure 4a), which is only possible for the minor gg conformer. This conclusion was further confirmed by 1D NOESY experiments with selection of the resonance of H4′ (see the Supporting Information).

Proton H5′ and both H6′ protons in the ^{1}H NMR spectrum of the α(5→6′) *O*-linked analogue **10** were isochronous, precluding the measurement of the corresponding vicinal *J*(5′,6′) coupling constants. Consequently, in this case, the description of the conformational equilibrium relied exclusively upon the observation of key NOE cross peaks in the NOESY experiments. A very strong NOE was observed between H5 and H6′ protons, but it was not possible to discriminate in terms of intensities between both geminal protons of the hydroxymethyl group. Neither was it possible to discriminate an observable NOE between H8a at the iminosugar moiety and H5′ or either H6′ protons at the glucopyranosyl ring, which prevented experimental confirmation of the ψ 180° conformer. On the other hand, two clear NOE contacts were observed between H8a and H4′, as well as between H7 and H4′, which corroborated the contribution of the gg conformer around the C5′–C6′ linkage.

In the case of the *S*-linked isomaltoside **11**, the H6′(*proR*) proton showed a significantly stronger NOE with H4′ than with H6′(*proS*), indicating a situation similar to that described above for **12**, corroborating the prevalence of the gt rotamer at the ω torsion. The signal dispersion on the spectrum in this case was much higher than for the *O*-linked derivative **10** and allowed the detection of a significant NOE contact between H5 at the piperidine ring and H5′ at the glucopyranose aglycone, revealing the presence of conformers with values around 90° for the ψ torsion.

The distributions of conformers around the α(5→4′) pseudoglycosidic linkages in the maltoside mimics **13**–**15** can be fundamentally described by the observation of key NOE contacts between proton H5 on the iminosugar ring and

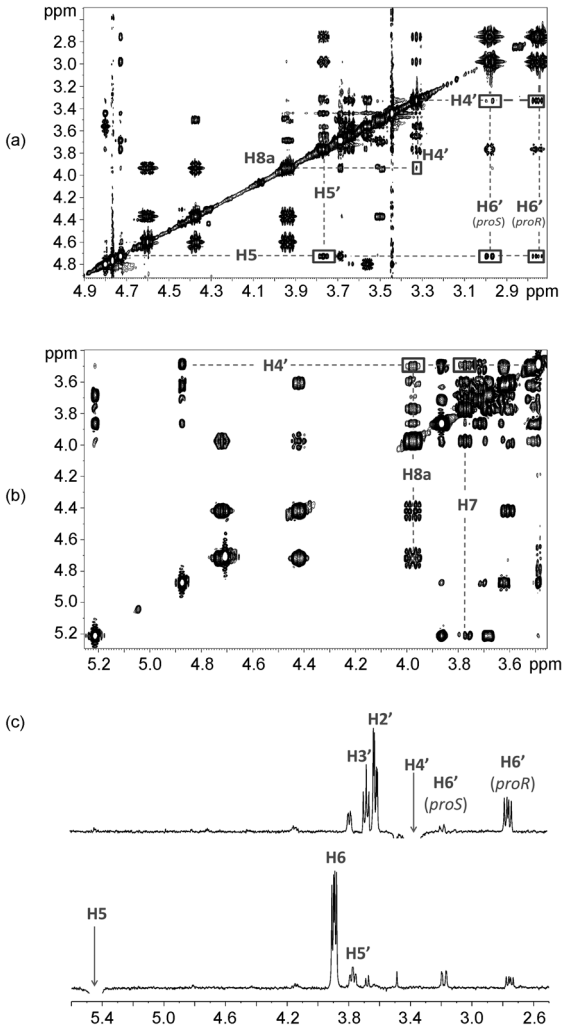

Figure 4. NOE experiments for a) **12**, b) **10**, and c) **11**. 2D NOESY experiments are shown for **12** and **10** (500 MHz, 400 ms mixing time; at 25 and 35 °C, respectively). In the case of **11**, which exhibited a much better spectral dispersion, 1D NOESY experiments are shown (500 MHz, 35 °C, 2 s mixing time), with selection of H5 (bottom row) or H4′ (top row) protons. Key NOESY cross peaks are highlighted on each spectrum. See the Supporting Information for a color version of this figure.

other protons in the aglycone glucose moiety, particularly H4′, H3′, and H5′. All the compounds showed very strong H5–H4′ NOE contacts, which is indicative of major contributions of *syn*ϕ–*syn*ψ conformations in solution (Figure 5a and Figure 6). For **13** and **15**, very weak NOE contacts correlating H5 with H3′ and H5′ could be observed (Figure 5b and Figure 6b), however, they were only observable at large NOESY mixing times (800 ms), so spin diffusion through H4′ and H3′ could not be safely ruled out. These weak NOE contacts would be indicative of a certain degree of flexibility around the *syn*ϕ–*syn*ψ region of the energy map (see below).

In the case of the *S*-linked pseudomaltoside **14**, the NOESY spectra showed a NOE correlation between proton H8a in the sp^2-iminosugar ring and proton H3′ in the aglycone glucose residue (Figure 6c). The similarity of molecu-

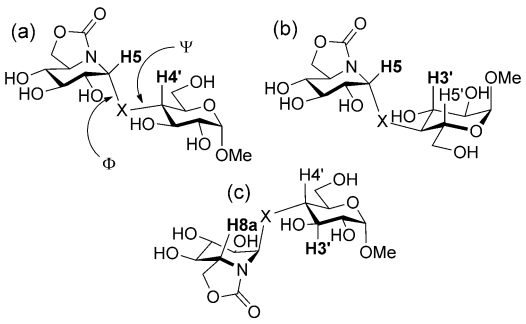

Figure 5. Schematic representation of the major conformers identified by NOESY spectra for the maltoside mimics. Structure c), detected only in the case of the *S*-linked derivative **14**, represents a *synϕ–antiψ* conformation. Protons involved in diagnostic NOE contacts are depicted. Key NOEs for each conformation, as discussed in the text, are highlighted in bold.

lar sizes and chemical structure of all the three α(5→4′) linked pseudodisaccharides precluded any possible spin diffusion effects present only in the case of **14**. On the other hand, the S atom has the largest covalent radius among N, O, and S, which leads to larger inter-residual distances and, hence, lower inter-residual NOEs, reducing the probability of spin diffusion for **14**, in comparison with **13** or **15**. Most probably, the observed H8a/H3′ inter-residual NOE is reporting on particular conformational characteristics around the *S*-pseudoglycosidic linkage (Figure 5c).

The remaining NOE cross peaks observed in the NOESY spectra of **13**–**15** report trivial intraresidual spatial contacts for the two six-membered rings. On the other hand, vicinal $J(5',6')$ coupling constants could be estimated from the 1D ^{1}H NMR spectra. They define the conformations of the exocyclic hydroxymethyl groups at the glucopyranose rings of the pseudodisaccharides. The experimental values were around 2.0–2.5 and 4.0–5.0 Hz, in agreement with a typical equilibrium distribution of rotamers around the ω torsion angle of about 70:30 gg/gt for D-glucopyranose derivatives,[37] without any clear contribution of the tg conformer. This result is particularly relevant in the case of **15** because it indicates that protonation of the amino group at the pseudoglycosidic linkage, which is expected to occur at physiological pH, does not induce any perceivable conformational shift of the hydroxymethyl group of the aglycone residue.

Molecular modeling: The energy minima obtained for the α-(5→6′)-linked pseudodisaccharides **10**–**12** are represented as stick models, along with the probability maps, in Figure 7. The pseudothioisomaltoside **11** showed an energy preference towards the gt conformer around the ω torsion, in perfect agreement with the NMR observations. The predicted minimum at ψ 90° (Figure 7a) was highly populated in solution, as indicated by the strong H5/H5′ NOE (Figure 4c). The observation of H5-H6′ NOEs revealed the presence of conformers in the *anti-ψ* region (ψ 180°), but in lower relative proportions than the previous minimum. For the *N*-linked analogue **12**, the situation was rather similar to that with **11**, showing two major conformations with ψ 180° or

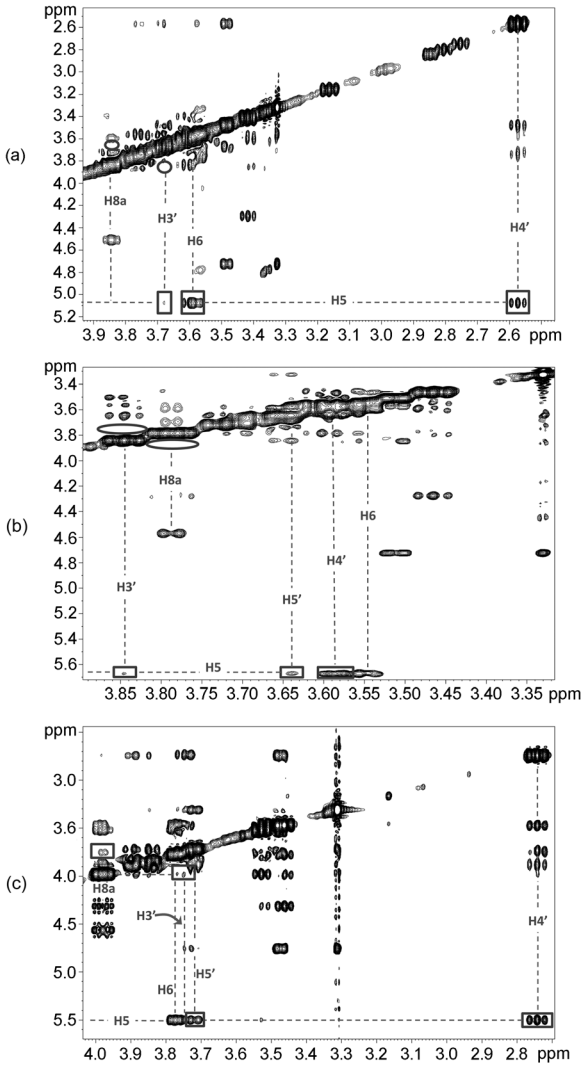

Figure 6. NOESY spectra of a) **15**, b) **13**, and c) **14** (500 MHz, 25 °C, 800 ms mixing time). Key NOESY cross peaks are highlighted on each spectrum. Only **14** showed a NOE cross peak between proton H8a at the sp^2-iminosugar moiety and H3′ of the glucopyranose ring. Circles on a) and b) highlight the absence of the H8a/H3′ cross peaks in the NOESY spectra of **15** and **13**. See the Supporting Information for a color version of this figure.

90°. Although all the identified minima in the adiabatic map of **12** were gt conformers around ω, the observation of a weak H8a–H4′ NOE (Figure 4a) was indicative of the presence of the gg conformer in solution. This discrepancy can be attributed to deficiencies inherent to the force field approach, which seems to be able to identify only the most stable conformer around a very flexible linkage, not reproducing well the less populated conformational states.

The strong intensity of the H5/H6′ NOE in the NOESY spectrum of the *O*-linked pseudoisomaltoside **10** (no stereospecific distinction was possible in this case) indicated a major contribution from the ψ 180° conformer. Interestingly, in this case, the molecular modelling protocol led to the prediction of energetically favorable gg conformers besides the gt conformers (Figure 7c), which was in very good

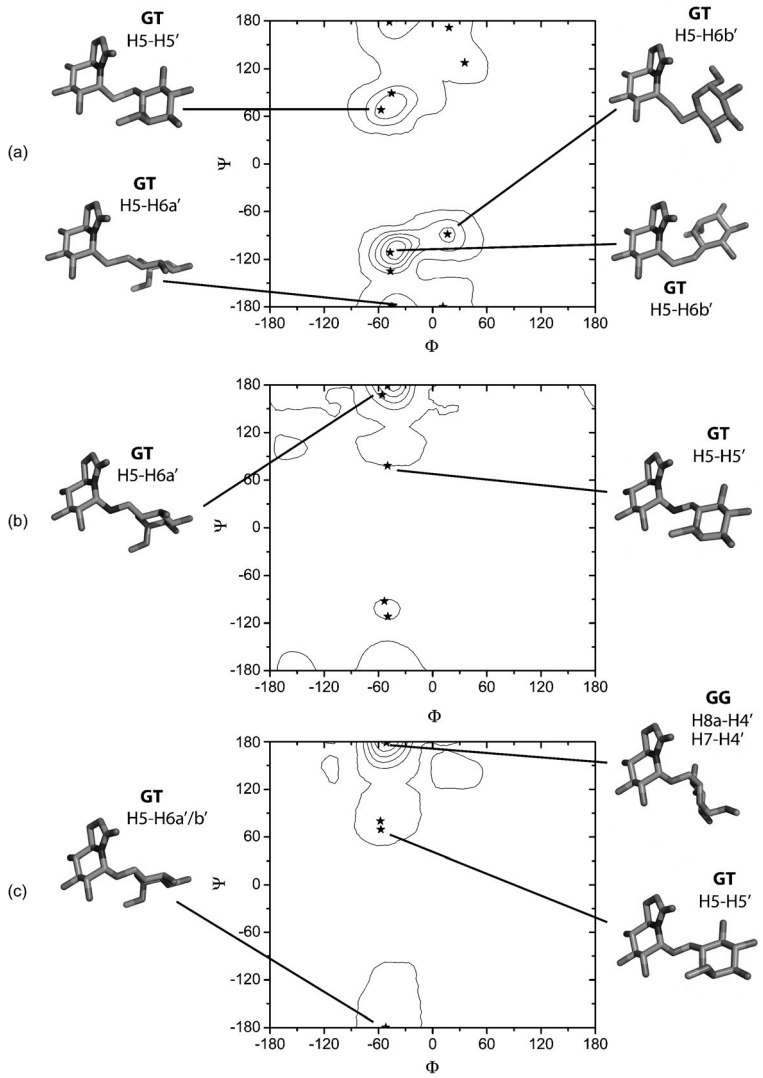

Figure 7. Molecular modeling of the α(5→6′)-linked disaccharide mimics. The probability maps at 25 °C of a) **11**, b) **12**, and c) **10** obtained from the corresponding adiabatic maps (see the Supporting Information) are shown. Solid lines cover those ϕ,ψ regions of the conformational space showing 20, 10, 1, and 0.1 % of the total conformer populations. The most populated solutions from Monte Carlo calculations are represented in stick diagrams. The observed NOEs characterizing these conformations are also indicated. See the Supporting Information for a color version of this figure.

agreement with the experimental observations of the H8a/H4′ and H7/H4′ NOE contacts.

Together, the combined protocol (NMR and molecular modeling) for the α(5→6′)-linked pseudodisaccharides indicated a rather similar conformational behavior of the three molecules in solution, with only very subtle differences in terms of major populations (ψ 90° for **11** and **12**, and ψ 180° for **10**). In any case, all three compounds showed significant flexibility around the ω and ψ torsions of their pseudoglycosidic linkages. The scenario is actually analogous to that encountered for the α(1→6′)-linked parent disaccharide isomaltose.[38]

The probability maps of the pseudoglycosidic torsion angles ϕ and ψ for the maltoside mimics **13**–**15**, obtained from the corresponding adiabatic maps, are shown in Figure 8. Along with the probability isocontour levels, isodistance curves for the H5–H4′ and H8a–H3′ distances are represented. All ϕ,ψ values within the area of these curves should lead to the experimental observation of a cross peak in the NOESY spectra correlating the two protons defining the curve. These two distances were monitored in the graphs because they are characteristically within NOE observation distance for the two main regions of the ϕ,ψ map, namely the *syn*ϕ–*syn*ψ and *syn*ϕ–*anti*ψ regions, respectively. The *anti*ϕ–*anti*ψ region can be discarded from the molecular modeling calculations on energy grounds. These two distances were then considered for an analysis based on "exclusive NOEs".

The molecular models representative of the minima obtained by the Monte Carlo protocol are represented on the probability maps in Figure 8. For each solution, the expected key interresidual NOEs are also indicated. The predicted distances for those NOEs that could unambiguously be observed and quantified in the NMR spectra were calculated from the output structures of the MC/SD and the MC/SD/MM calculations, respectively, and are included in Table 1. As typically found for carbohydrate structures, very few NOEs of sufficient quality were available for the determination of the structures, nevertheless those collected in Table 1 were in rather good agreement with the resulting molecular models from the Monte Carlo calculations.

The combined analysis of NMR and modeling data provide important information on the differential conformation behavior of the aglycone moiety in these α(5→4′)-linked pseudodisaccharides depending on the type of electronegative atom connecting the two six-membered rings (S, N, or O). For the *N*-linked maltoside mimetic **15**, the accessible conformations are restricted to a relatively well-defined narrow area of the energy map, centred on *syn*-ψ values with $\phi<0$ and $\psi<0$. For the *O*-linked derivative **13**, the ad-

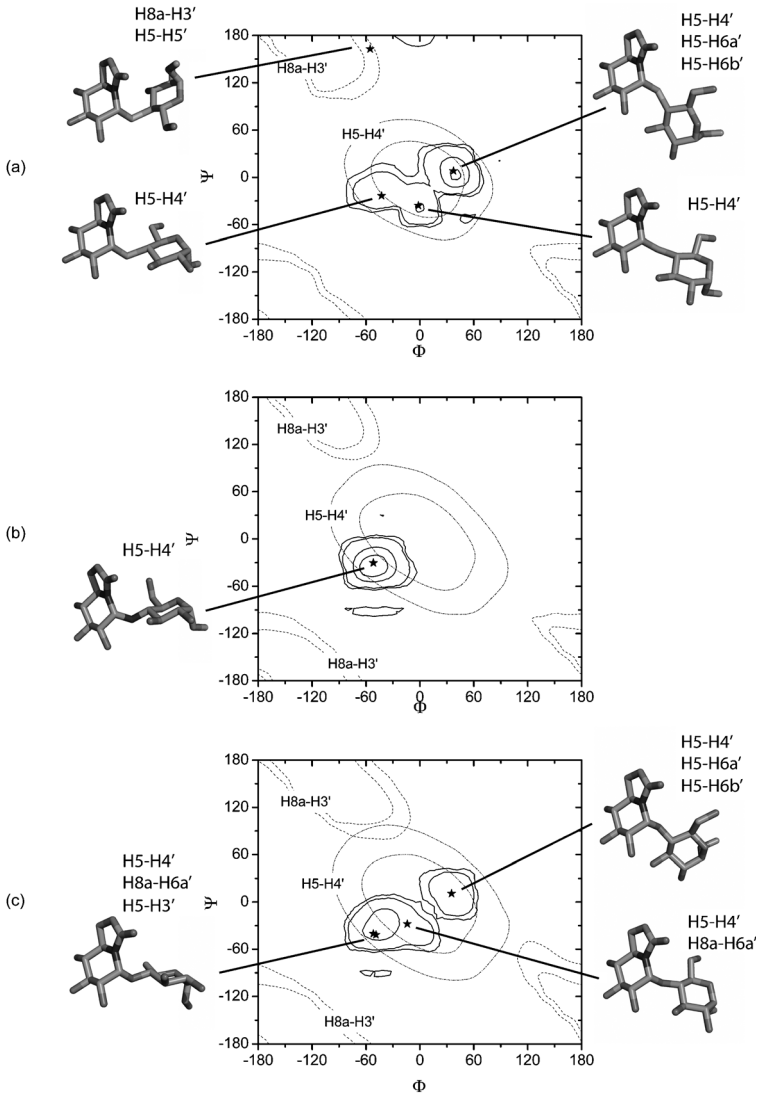

Figure 8. Molecular modeling of the α(5→4′)-linked disaccharide mimics. The probability maps at 25°C of compounds a) **14**, b) **15**, and c) **13**, obtained from the corresponding adiabatic maps (see the Supporting Information) are shown. Solid lines cover those ϕ,ψ regions of the conformational space showing 20, 10, 1, and 0.1% of the total conformer populations. Dashed lines show relevant interproton distances represented in levels between 2.0 and 3.0 Å. The most populated solutions from Monte Carlo calculations are represented in stick diagrams. The observed NOEs characterizing these conformations are also indicated. See the Supporting Information for a color version of this figure.

Table 1. Relevant interproton distances [Å] defining the conformations of the α(5→4′) pseudodisaccharides **13**–**15**.

		H5–H4′	H5–H3′
15	MC/SD[a]	2.59	3.57
	MC/SD + MM[b]	2.68	3.59
	experimental[c]	2.70	3.60
13	MC/SD	2.54	3.28
	MC/SD + MM	2.53	3.4
	experimental	2.46	3.35
14	MC/SD	2.39	3.84
	MC/SD + MM	2.36	4.21
	experimental	2.42	–

[a] Monte Carlo Simulation and Stochastic Dynamics. [b] MC/SD followed by Multiple Minimization. [c] From initial growth rates of 1D NOESY build-up curves and applying the isolated spin pair approximation (ISPA).

jacent region within the *syn*-ψ area ($\phi>0$, $\psi>0$) is also accessible, reflecting some increased flexibility around the pseudoglycosidic linkage in comparison to **15**, a situation that is rather similar to that encountered for the parent α(1→4)-linked disaccharide maltose.[38a,39] For the *S*-linked derivative **14**, besides a *syn*-ψ region similar to that accessible to the *O*-derivative, the computational procedure predicted a lower probability for a conformation in the *anti*-ψ region (ψ around 180°). Indeed, for this molecule, a NOE cross peak of significant intensity could be observed between protons H8a and H3′. This NOE, which is an exclusive NOE contact for the *syn*ϕ–*anti*ψ region, was absent from the NOESY spectra of **13** and **15** (Figure 6). Indeed, the situation is analogous to that encountered for methyl 4-thio-α-maltoside in comparison with methyl α-maltoside.[40]

The differential behavior of the aglycones as a function of the linking heteroatom can be interpreted in terms of the respective covalent radii. Thus, the much larger covalent radius of sulfur in comparison to nitrogen and oxygen, leads to larger distances between the two constituent rings, reducing significantly the steric barrier needed to overcome any *syn*$\psi\leftrightarrow$ *anti*ψ transition and facilitating adoption of these higher energy conformations, as experimentally observed for **14**. Some differences were also observed between the *N*- and *O*-linked derivatives **13** and **15**, even when the intersaccharide atoms (O and N, respectively) have similar covalent radii. The more restricted accessibility of the *N*-linked derivative **15** to the conformational map might be a result of the local electrostatic field due to the net positive charge that is present in the protonated form of the pseudoglycosidic linkage, which is the major species present at physiological pH.

Conformational behavior–glycosidase inhibitory activity relationships: Inhibition of isomaltase and maltase by the new linkage-spanning pseudodisaccharide inhibitors was of the competitive type. Kinetics experiments modifying the incu-

bation time revealed that they are fast-binding inhibitors, suggesting that no deep conformational changes take place upon formation of the enzyme–inhibitor complex. Most probably, the enzyme, in its ground-state conformation, binds the inhibitor in one of its accessible conformations in solution. The available crystallographic and molecular modeling information on the complexes of isomaltase[41] and maltase[42] with their substrates/inhibitors suggests that most of the enthalpic contribution to binding comes from interactions involving the glycone moiety with amino acid residues at the −1 site. In the case of isomaltoside analogues, the D-glucopyranosyl aglycone unit probably retains substantial flexibility about the three-covalent-bond segment connecting the piperidine and the pyranose ring upon complexation, thereby limiting the entropic penalty of binding.[43] The almost identical inhibition constants of the isomaltoside mimetics **10**–**12** against isomaltase (Table 2) is in agreement with this assumption and means that no significant stabilizing effects occur due to electrostatic interactions involving the amino group in the case of the N-linked derivative **12**. The inhibition of maltase evidenced some small differences (less than one order of magnitude) with inhibition potencies that decreased with the trend **10** > **12** > **11**, which most likely indicates a different mode of recognition (Table 2).

Table 2. Inhibition constants (K_i [μM]) for the pseudodisaccharides **10**–**15**.[a,b]

Enzyme	**12**	**10**	**11**	**15**	**13**	**14**
β-glucosidase/galactosidase (bovine liver)	195	n.i.	n.i.	190	n.i.	n.i.
β-glucosidase (almonds)	n.i.	n.i.	n.i.	375	n.i.	209
maltase (yeast)	17	5.5	30	108	24	n.i.
isomaltase (yeast)	53	55	52	83	36	n.i.
trehalase (pig kidney)	549	n.i.	n.i.	n.i.	n.i.	n.i.
naringinase (Penicillium decumbes)	742	702	187	443	160	n.i.

[a] Inhibition was competitive in all cases. [b] No inhibition (n.i.) at 1 mM concentration was observed for any of the new compounds against α-mannosidase (Jack beans), β-mannosidase (*Helix pomatia*), α-galactosidase (green coffee beans), β-galactosidase (*E. coli*), and amyloglucosidase (*Aspergillus niger*).

In the case of maltoside mimetics **13**–**15** (Table 2), having a two-covalent-bond spacer between the (pseudo)monosaccharide constituents, the scenario was totally different. Most probably, in this case, enzyme binding involves a defined conformation about the ϕ and ψ dihedral angles. Although binding of different conformers depending on the interglycosidic heteroatom cannot be discarded, the penalty of freezing a given conformation will be lower if it is already highly populated in solution and will increase with molecular flexibility. The significantly higher inhibition potency of the *O*-linked maltoside mimic **13** compared with the more rigid *N*-linked analogue **15**, especially in the case of maltase, might then be ascribed to a lower accessibility of the bound conformation when replacing the intersaccharide oxygen by ammonium. Moving from oxygen to sulfur in this series had even more dramatic consequences. Thus, among the six compounds studied, compound **14** was the only one that showed no ability for inhibition of either isomaltase or maltase. The inability of α-mannosidase to accommodate thio-substituted glycosides analogous to the natural oligosaccharide substrates has previously been noted.[44] It was speculated that increased rigidity might be at the origin of this observation. However, our data indicate that the most stable unbound conformations for the *O*-linked homologue **13** are also significantly populated in the case of **14** and, indeed, support a higher conformational flexibility for the latter, in line with other studies on thioligosaccharides.[45] It is likely that the increased flexibility around the longer *S*-pseudoglycosidic linkage of **14** results in a much stronger entropic penalty for the binding process in comparison with **13** or **15**, which have structurally better defined conformations in the unbound state.

Conclusion

The present results support the potential of sp^2-iminosugars as building blocks for the construction of stable pseudo *O*-, *S*-, and *N*-oligosaccharide mimetics. Their unique stereoelectronic characteristics allow access to unprecedented α-linked derivatives in which the acetal functional group characteristic of natural glycosidic linkages is replaced by chemically and enzymatically stable aminoacetal, aminothioacetal or *gem*-diamine functionalities. The analogy between those groups makes the approach very attractive for the design of homologous series of linkage-spanning inhibitors of glycosidases acting on oligosaccharides for structure–activity relationship studies. We have carried out this exercise for isomaltose and maltose pseudodisaccharides. The inhibitory activities towards isomaltase and maltase, two enzymes that bind isomaltose and maltose either as substrate or inhibitor, were correlated with their conformational behavior in solution as determined by NMR and molecular modeling. The three isomaltose mimics exhibited conformational properties very similar to those of the parent disaccharide, which translated into very selective inhibition of the two enzymes with small differences depending upon the linking heteroatom. In stark contrast, the *O*-, *N*-, and *S*-linked maltose mimics significantly differed in their conformational flexibility as well as in their isomaltase and maltase inhibitory potency. Thus, the *O*-pseudodisaccharide, which matched the conformational characteristics of maltose, was a potent and very selective inhibitor of both enzymes. The inhibitory activity was greatly reduced for the more rigid N-linked analogue, and was fully abolished for the much more flexible thiomaltoside homologue, thereby illustrating the utmost importance of incorporating conformational considerations in the design of aglycone-selective glycosidase inhibitors.

Experimental Section

General Methods: Reagents and solvents were purchased from commercial sources and used without further purification, except for dichloromethane, which was distilled under an Ar stream over CaH_2. Optical rotations were measured at 20 °C in 1 cm or 1-dm tubes with a Perkin–Elmer 141 MC polarimeter. IR spectra were recorded with a JASCO FTIR-4100 (ATR) spectrometer. ^{1}H and ^{13}C NMR spectra were recorded at 500 (125.7) and 300 (75.5) MHz with Bruker AVANCE DRX 500 and 300 spectrometers. 2D COSY, 1D TOCSY, and HMQC experiments were used to assist NMR assignments. Thin-layer chromatography (TLC) was carried out on aluminium sheets coated with Kieselgel 30 F245 (E. Merck), with visualisation by UV light and by charring with 10 % H_2SO_4 or 0.1 % ninhydrin in EtOH. Column chromatography was carried out on Silica Gel 60 (E. Merck, 230–400 mesh). Electrospray mass spectra (ESIMS) were obtained with a Bruker Esquire6000 instrument. Elemental analyses were performed at the Instituto de Investigaciones Químicas (Sevilla, Spain). The glycosidases α-glucosidase (from yeast), β-glucosidase (from almonds), β-glucosidase/β-galactosidase (from bovine liver, cytosolic), α-galactosidase (from green coffee beans), isomaltase (from yeast), trehalase (from pig kidney), amyloglucosidase (from *Aspergillus niger*), α-mannosidase (from jack bean), β-mannosidase (from *Helix pomatia*), β-galactosidase (from *E. coli*) used in the inhibition studies, as well as the corresponding *o*- and *p*-nitrophenyl glycoside substrates were purchased from Sigma Chemical Co.

Synthesis: The starting materials, (5*R*,6*R*,7*S*,8*R*,8a*R*)-5,6,7,8-tetra-*O*-acetyl-2-oxa-3-oxoindolizidine (**16**), methyl 2,3,4-tri-*O*-acetyl-α-D-glucopyranoside (**18**),[27] methyl 2,3,6-tri-*O*-acetyl-α-D-glucopyranoside (**20**),[28] 2,3,4-tri-*O*-acetyl-6-thio-α-D-glucopyranoside (**22**),[29] methyl 6-amino-6-deoxy-α-D-glucopyranoside (**27**),[32] and methyl 4-amino-4-deoxy-α-D-glucopyranoside (**28**)[33] were prepared as described previously. Methyl 2,3,6-tri-*O*-benzoyl-4-thio-α-D-glucopyranoside (**24**)[30] was prepared from methyl 2,3,6-tri-*O*-benzoyl-4-*O*-trifluoromethanesulfonyl-α-D-galactopyranoside[30] by S_N2 displacement of the triflate group by potassium thioacetate and final *S*-deacetylation with hydrazine.[47]

(5*R*,6*R*,7*S*,8*R*,8a*R*)-6,7,8-Triacetoxy-5-fluoro-2-oxa-3-oxoindolizidine (17): Compound **16** (560 mg, 1.50 mmol) and HF-pyridine (70 %, 2.8 mL) were placed in a polyethylene vessel cooled at −40 °C. The reaction mixture was stirred at this temperature for 80 min, diluted with Et_2O (30 mL), washed with saturated aqueous KF (15 mL) and extracted with Et_2O (3×30 mL). The organic layer was washed with saturated aqueous $NaHCO_3$ (10 mL), dried (Na_2SO_4) and concentrated. The resulting residue was purified by flash chromatography (1:2 EtOAc/petroleum ether). Yield: 300 mg (60 %); amorphous solid; R_f = 0.77 (2:1 EtOAc/petroleum ether); $[\alpha]_D$ = +21.6 (c = 0.9 in $CHCl_3$); ^{1}H NMR (500 MHz, $CDCl_3$): δ = 6.17 (dd, J(5,F) = 52.5 Hz, J(5,6) = 3.5 Hz, 1H; H-5), 5.60 (t, J(6,7) = J-(7,8) = 10.0 Hz, 1H; H-7), 5.00 (ddd, J(5,6)=3.5 Hz, J(6,7)=10.0 Hz, J-(6,F) = 14.0 Hz, 1H; H-6), 4.99 (t, J(7,8) = J(8,8a) = 10.0 Hz, 1H; H-8), 4.51 (dd, J(1a,1b) = 9.0 Hz, J(1a,8a) = 8.0 Hz, 1H; H-1a), 4.32 (t, J-(1a,1b) = J(1b,8a) = 9.0 Hz, 1H; H-1b), 4.17–4.09 (m, 1H; H-8a), 2.15–2.09 ppm (3 s, 9H; *Me*CO); ^{13}C NMR (125.7 MHz, $CDCl_3$): δ = 170.0–169.5 (Me*CO*), 154.2 (CO), 87.5 (C-5, d, J(C5,F) = 211.6 Hz), 72.0 (C-8), 69.8 (C-6, d, J(C6,F) = 24.8 Hz), 68.6 (C-7), 67.2 (C-1), 52.0 (C-8a), 20.4 (*Me*CO); MS (ESI): m/z: 356.1 $[M+Na]^+$; elemental analysis calcd (%) for $C_{13}H_{16}NO_8F$: C 46.85, H 4.84, N 4.20; found: C 46.77, H 4.71, N 4.02.

(5*R*,6*R*,7*S*,8*R*,8a*R*)-6,7,8-Tri-*O*-acetyl-5-(methyl 2,3,4-tri-*O*-acetyl-α-D-glucopyranosid-6-yl)-2-oxa-3-oxoindolizidine (19): BF_3.OEt_2 (15 μL, 0.10 mmol) was added to a stirred solution of **17** (70 mg, 0.21 mmol) and **18** (67 mg, 0.21 mmol) in anhydrous CH_2Cl_2 (2 mL) at 0 °C under a nitrogen atmosphere. The mixture was stirred for 30 min, diluted with CH_2Cl_2 (25 mL), washed with saturated aqueous $NaHCO_3$ (5 mL), dried (Na_2SO_4) and concentrated. The resulting residue was purified by flash chromatography (2:3→1:1 EtOAc/petroleum ether). Yield: 85 mg (64 %); amorphous solid; R_f = 0.31 (1:1 EtOAc/petroleum ether); $[\alpha]_D$ = +97.6 (c = 1.0 in $CHCl_3$); ^{1}H NMR (500 MHz, $CDCl_3$): δ = 5.56 (t, J(6,7) = J(7,8) = 9.5 Hz, 1H; H-7), 5.49 (t, J(2′,3′) = J(3′,4′) = 9.5 Hz, 1H; H-3′), 5.45 (d, J(5,6) = 4.0 Hz, 1H; H-5), 5.09 (t, J(3′,4′) = J(4′,5′) = 9.5 Hz, 1H; H-4′), 4.96 (d, J(1′,2′) = 3.5 Hz, 1H; H-1′), 4.94 (t, J(7,8) = J(8a,8) = 9.5 Hz, 1H; H-8), 4.89 (dd, J(5,6) = J(8a,8) = 9.5 Hz, 1H; H-6), 4.87 (dd, J(1′,2′) = 3.5 Hz, J(2′,3′) = 9.5 Hz, 1H; H-2′), 4.48 (t, J(1a,1b) = J(1a,8a) = 9.0 Hz, 1H; H-1a), 4.25 (dd, J(1a,1b) = 9.0 Hz, J(1b,8a) = 7.5 Hz, 1H; H-1b), 4.13 (dt, J(1a,8) = J(8,8a) = 9.0 Hz, J(1b,8a) = 7.5 Hz, 1H; H-8a), 3.92 (ddd, J(4′,5′) = 9.5 Hz, J(5′,6b′) = 4.5 Hz, J(5′,6a′) = 3.0 Hz, 1H; H-5′), 3.69 (dd, J(5′,6a′) = 3.0 Hz, J(6a′,6b′) = 11.0 Hz, 1H; H-6a′), 3.66 (dd, J-(5′,6b′) = 4.5 Hz, J(6a′,6b′) = 11.0 Hz, 1H; H-6b′), 3.45 (s, 3H; OMe), 2.13–2.03 ppm (6 s, 18H; *Me*CO); ^{13}C NMR (125.7 MHz, $CDCl_3$): δ = 170.2–169.6 (Me*CO*), 155.8 (CO), 96.6 (C-1′), 79.1 (C-5), 72.7 (C-8), 70.8–70.4 (C-2′, C-6), 70.2 (C-3′), 69.1 (C-7), 68.6 (C-4′), 67.9 (C-5′), 67.4 (C-6′), 66.8 (C-1), 55.4 (OMe), 51.6 (C-8a), 20.7–20.5 ppm (*Me*CO); MS (ESI): m/z: 656.2 $[M+Na]^+$; elemental analysis calcd (%) for $C_{26}H_{35}NO_{17}$: C 49.29, H 5.57, N 2.21; found: C 49.37, H 5.40, N 2.08.

Oxa-3-oxoindolizidine (10): Compound **10** was obtained by conventional de-*O*-acetylation of **19** (50 mg, 0.08 mmol) with catalytic NaOMe in MeOH. Yield: 27.5 mg (91 %); R_f = 0.64 (6:3:1 MeCN/H_2O/NH_4OH); $[\alpha]_D$ = +68.7 (c = 0.6 in H_2O); ^{1}H NMR (500 MHz, D_2O): δ = 5.09 (d, J-(5,6) = 4.0 Hz, 1H; H-5), 4.75 (d, J(1′,2′) = 3.5 Hz, 1H; H-1′), 4.60 (t, J-(1a,1b) = J(1a,8a) = 9.0 Hz, 1H; H-1a), 4.30 (dd, J(1a,1b) = 9.0 Hz, J-(1b,8a) = 6.5 Hz, 1H; H-1b), 3.85 (ddd, J(1a,8) = 9.0 Hz, J(8a,8) = 9.5 Hz, J(1b,8a) = 6.5Hz, 1H; H-8a), 3.77–3.71 (m, 3H; H-5′, H-6a′, H-6b′), 3.65 (t, J(6,7) = J(7,8) = 9.5 Hz, 1H; H-7), 3.59 (t, J(2′,3′) = J(3′,4′) = 9.5 Hz, 1H; H-3′), 3.57 (dd, J(5,6) = 4.0 Hz, J(6,7) = 9.5 Hz, 1H; H-6), 3.50 (dd, J-(1′,2′) = 3.5 Hz, J(2′,3′) = 9.5 Hz, 1H; H-2′), 3.49 (t, J(7,8) = J(8a,8) = 9.5 Hz, 1H; H-8), 3.43–3.35 (m, 1H; H-4′), 3.36 ppm (s, 3H; OMe); ^{13}C NMR (125.7 MHz, D_2O): δ = 158.4 (CO), 99.4 (C-1′), 81.3 (C-5), 73.5 (C-8), 73.3 (C-3′), 72.5 (C-7), 71.2 (C-2′), 71.0 (C-6), 70.0 (C-5′), 69.4 (C-4′), 67.6 (C-1), 66.2 (C-6′), 55.2 (OMe), 53.1 ppm (C-8a); MS (ESI): m/z: 404.1 $[M+Na]^+$; elemental analysis calcd (%) for $C_{14}H_{23}NO_{11}$: C 44.10, H 6.08, N 3.67; found: C 43.97, H 6.02, N 3.42.

(5*R*,6*R*,7*S*,8*R*,8a*R*)-6,7,8-Triacetoxy-5-(methyl 2,3,6-tri-*O*-acetyl-α-D-glucopyranosid-4-yl)-2-oxa-3-oxoindolizidine (21): BF_3.OEt_2 (15 μL, 0.10 mmol) was added to a stirred solution of **17** (70 mg, 0.21 mmol) and **20** (67 mg, 0.21 mmol) in anhydrous CH_2Cl_2 (2 mL) at 0 °C under a nitrogen atmosphere. The mixture was stirred for 30 min, diluted with CH_2Cl_2 (25 mL), washed with saturated aqueous $NaHCO_3$ (5 mL), dried (Na_2SO_4) and concentrated. The resulting residue was purified by flash chromatography (1:2 EtOAc/petroleum ether). Yield: 65 mg (65 %); amorphous solid; R_f = 0.62 (2:1 EtOAc/petroleum ether); $[\alpha]_D$ = +80.8 (c = 1.0 in $CHCl_3$); ^{1}H NMR (500 MHz, $CDCl_3$): δ = 5.73 (d, J(5,6) = 4.5 Hz, 1H; H-5), 5.54 (dd, J(2′,3′) = 10.0 Hz, J(3′,4′) = 9.0 Hz, 1H; H-3′), 5.43 (t, J(6,7) = J(7,8) = 10.0 Hz, 1H; H-7), 4.89 (t, J(8,8a) = 10.0 Hz, 1H; H-8), 4.87 (d, J(1′,2′) = 4.0 Hz, 1H; H-1′), 4.86 (dd, J(5,6) = 4.5 Hz, J-(6,7) = 10.0 Hz, 1H; H-6), 4.80 (dd, J(1′,2′) = 4.0 Hz, J(2′,3′) = 10.0 Hz, 1H; H-2′), 4.43 (t, J(1a,1b) = J(1a,8a) = 9.0 Hz, 1H; H-1a), 4.31 (br s, 1H; H-6a′), 4.30 (br s, 1H; H-6b′), 4.22 (dd, J(1a,1b) = 9.0 Hz, J(1b,8a) = 7.5 Hz, 1H; H-1b), 4.07 (dd, J(3′,4′) = 9.0 Hz, J(4′,5′) = 10.0 Hz, 1H; H-4′), 3.96–3.87 (m, 2H; H-5′, H-8a), 3.42 (s, 3H; OMe), 2.16–2.03 ppm (6 s, 18H; *Me*CO); ^{13}C NMR (125.7 MHz, $CDCl_3$): δ = 171.4–169.6 (Me*CO*), 155.6 (CO), 96.8 (C-1′), 78.9 (C-5), 72.7 (C-3′), 72.5 (C-8), 72.2 (C-4′), 71.4 (C-2′), 69.4 (C-6), 68.4 (C-7), 67.2 (C-5′), 66.9 (C-1), 62.0 (C-6′), 55.5 (OMe), 52.1 (C-8a), 21.0–20.5 ppm (*Me*CO); MS (ESI): m/z: 656.2 $[M+Na]^+$; elemental analysis calcd (%) for $C_{26}H_{35}NO_{17}$: C 49.29; H 5.57; N 2.21; found: C 49.19; H 5.42; N 2.10.

(5*R*,6*R*,7*S*,8*R*,8a*R*)-6,7,8-Trihydroxy-5-(methyl α-D-glucopyranosid-4-yl)-2-oxa-3-oxoindolizidine (13): Compound **13** was obtained by conventional de-*O*-acetylation of **21** (50 mg, 0.08 mmol) with catalytic NaOMe in MeOH. Yield: 26.2 mg (87 %); amorphous solid; R_f = 0.57 (6:3:1 MeCN/H_2O/NH_4OH); $[\alpha]_D$ = +99.9 (c = 0.5 in H_2O); ^{1}H NMR (500 MHz, D_2O): δ = 5.68 (d, J(5,6) = 4.0 Hz, 1H; H-5), 4.73 (d, J(1′,2′) = 4.0 Hz, 1H; H-1′), 4.58 (t, J(1a,1b) = J(1a,8a) = 9.0 Hz, 1H; H-1a), 4.28 (dd, J(1b,8a) = 6.0 Hz, 1H; H-1b), 3.85 (t, J(2′,3′) = J(3′,4′) = 9.5 Hz, 1H; H-3′), 3.79 (td, J(8a,8) = 9.0 Hz, 1H; H-8a), 3.74 (dd, J(6a′,6b′) = 11.5 Hz, J(5′,6a′) = 2.0 Hz, 1H; H-6a′), 3.71–3.63 (m, 2H; H-5′, H-6b′), 3.59 (t, J(6,7) = J-(7,8) = 9.5 Hz, 1H; H-7), 3.58 (t, J(3′,4′) = J(4′,5′) = 9.5 Hz, 1H; H-4′), 3.55 (dd, J(5,6) = 4.5 Hz, J(6,7) = 10.0 Hz, 1H; H-6), 3.50 (dd, J(1′,2′) = 4.0 Hz, J(2′,3′) = 10.0 Hz, 1H; H-2′), 3.47 (t, J(7,8) = J(8a,8) = 9.5 Hz, 1H; H-8), 3.34 ppm (s, 3H; OMe); ^{13}C NMR (125.7 MHz, D_2O): δ = 158.2

(CO), 99.2 (C-1′), 82.0 (C-5), 74.4 (C-4′), 73.9 (C-3′), 73.3 (C-8), 72.3 (C-7), 71.2 (C-2′), 70.9 (C-6), 69.7 (C-5′), 67.5 (C-1), 60.2 (C-6′), 55.0 (OMe), 53.5 ppm (C-8a); MS (ESI): *m/z*: 404.0 $[M+Na]^+$; elemental analysis calcd (%) for $C_{14}H_{23}NO_{11}$: C 44.10, H 6.08, N 3.67; found: C 43.86, H 5.84, N 3.39.

(5*R*,6*R*,7*S*,8*R*,8a*R*)-6,7,8-Triacetoxy-5-(methyl 2,3,4-tri-*O*-acetyl-6-thio-α-D-glucopyranosid-6-yl)-2-oxa-3-oxoindolizidine (23): $BF_3{\cdot}OEt_2$ (0.1 equiv) was added to a stirred solution of **17** (26 mg, 0.08 mmol) and **22** (40 mg, 0.12 mmol) in anhydrous CH_2Cl_2 (2 mL) at 0 °C under a nitrogen atmosphere. The mixture was stirred for 30 min, diluted with CH_2Cl_2 (25 mL), washed with saturated aqueous $NaHCO_3$ (5 mL), dried (Na_2SO_4) and concentrated. The resulting residue was purified by flash chromatography (1:2 EtOAc/petroleum ether). Yield: 42 mg (83%); R_f = 0.45 (2:1 EtOAc/petroleum ether); $[\alpha]_D$ = +90.6 (*c* = 0.7 in $CHCl_3$); ^{1}H NMR (500 MHz, $CDCl_3$): δ = 5.78 (d, *J*(5,6) = 6.0 Hz, 1H; H-5), 5.48 (t, *J*(2′,3′) = *J*(3′,4′) = 9.5 Hz, 1H; H-3′), 5.41 (t, *J*(6,7) = *J*(7,8) = 10.0 Hz, 1H; H-7), 5.09 (t, *J*(4′,5′) = 9.5 Hz, 1H; H-4′), 4.96 (dd, *J*(5,6) = 4.5 Hz, *J*(6,7) = 10.0 Hz, 1H; H-6), 4.93 (t, *J*(8,8a) = 10.0 Hz, 1H; H-8), 4.92 (d, *J*(1′,2′) = 3.5 Hz, 1H; H-1′), 4.87 (dd, *J*(1′,2′) = 3.5 Hz, *J*(2′,3′) = 9.5 Hz, 1H; H-2′), 4.55–4.49 (m, 1H; H-1a), 4.31–4.22 (m, 2H; H-1b, H-8a), 4.00 (ddd, *J*(4′,5′) = 9.5 Hz, *J*(5′,6b′) = 5.5 Hz, *J*(5′,6a′) = 3.5 Hz, 1H; H-5′), 3.45 (s, 3H; OMe), 3.04 (dd, *J*(5′,6a′) = 3.5 Hz, *J*(6a′,6b′) = 13.5 Hz, 1H; H-6a′), 2.66 (dd, *J*(5′,6b′) = 5.5 Hz, *J*(6a′,6b′) = 13.5 Hz, 1H; H-6b′), 2.13–2.02 ppm (6 s, 18H; *Me*CO); ^{13}C NMR (125.7 MHz, $CDCl_3$): δ = 170.2–169.4 (Me*C*O), 155.7 (CO), 96.6 (C-1′), 72.7 (C-8), 70.8 (C-2′), 70.5 (C-4′), 70.1 (C-6), 69.9 (C-3′), 69.6 (C-7), 68.0 (C-5′), 66.5 (C-1), 58.3 (C-5), 55.5 (OMe), 51.2 (C-8a), 31.2 (C-6′), 21.0–20.5 ppm (*Me*CO); MS (ESI): *m/z*: 672.2 $[M+Na]^+$; elemental analysis calcd (%) for $C_{26}H_{35}NO_{16}S$: C 48.07, H 5.43, N 2.16, S 4.94; found: C 47.98, H 5.35, N 2.01, S 4.76.

(5*R*,6*R*,7*S*,8*R*,8a*R*)-6,7,8-Trihydroxy-5-(methyl 6-thio-α-D-glucopyranosid-6-yl)-2-oxa-3-oxoindolizidine (11): Compound **11** was obtained by conventional de-*O*-acetylation of **23** (33 mg, 0.05 mmol) with catalytic NaOMe in MeOH. Yield: 18 mg (91%); R_f = 0.59 (6:3:1 MeCN/H_2O/NH_4OH); $[\alpha]_D$ = −16.0 (*c* = 0.4 in H_2O); ^{1}H NMR (500 MHz, D_2O): δ = 5.33 (d, *J*(5,6) = 5.5 Hz, 1H; H-5), 4.59 (t, *J*(1a,1b) = *J*(1a,8a) = 9.0 Hz, 1H; H-1a), 4.32 (dd, *J*(1a,1b) = 9.0 Hz, *J*(1b,8a) = 5.5 Hz, 1H; H-1b), 4.04 (td, *J*(1a,8) = *J*(8a,8) = 9.0 Hz, *J*(1b,8a) = 5.5 Hz, 1H; H-8a), 3.79 (dd, *J*(5,6) = 5.5 Hz, *J*(6,7) = 10.0 Hz, 1H; H-6), 3.67 (td, *J*(4′,5′) = *J*(5′,6b′) = 9.0 Hz, *J*(5′,6a′) = 2.5 Hz, 1H; H-5′), 3.60–3.54 (m, 2H; H-3′, H-7), 3.51 (dd, 1H, *J*(2′,3′) = 9.5 Hz, *J*(1′,2′) = 3.5 Hz, 1H; H-2′), 3.47 (t, *J*(7,8) = *J*(8a,8) = 9.0 Hz, 1H; H-8), 3.38 (s, 3H; OMe), 3.25 (t, *J*(3′,4′) = *J*(4′,5′) = 9.5 Hz, 1H; H-4′), 3.07 (dd, *J*(5′,6a′) = 2.6 Hz, *J*(6a′,6b′) = 14.0 Hz, 1H; H-6a′), 2.64 ppm (dd, *J*(5′,6b′) = 9.0 Hz, *J*(6a′,6b′) = 14.0 Hz, 1H; H-6b′); ^{13}C NMR (125.7 MHz, D_2O): δ = 157.9 (CO), 99.2 (C-1′), 73.5 (C-8), 73.2–72.9 (C-3′, C-7), 72.6 (C-4′), 71.3 (C-2′), 70.3 (C-6), 70.1 (C-5′), 67.3 (C-1), 61.3 (C-5), 55.0 (OMe), 52.8 (C-8a), 31.1 ppm (C-6′); MS (ESI): *m/z*: 420.1 $[M+Na]^+$; elemental analysis calcd (%) for $C_{14}H_{23}NO_{10}S$: C 42.31, H 5.83, N 3.52, S 8.07; found: C 42.15, H 5.71, N 3.25, S 7.84.

(5*R*,6*R*,7*S*,8*R*,8a*R*)-6,7,8-Triacetoxy-5-(methyl 2,3,6-tri-*O*-benzoyl-4-thio-α-D-glucopyranosid-4-yl)-2-oxa-3-oxoindolizidine (25): The α-*S*-linked pseudodissacharide **25** was obtained following the procedure described above using the fluoro-derivative **17** (73 mg, 0.22 mmol) and **24** (176 mg, 0.34 mmol). Column chromatography (1:2→1:1 EtOAc/petroleum ether). Yield: 115 mg (61%); amorphous solid; R_f = 0.66 (1:1 EtOAc/petroleum ether); $[\alpha]_D$ = +159.3 (*c* = 1.0 in $CHCl_3$); ^{1}H NMR (500 MHz, $CDCl_3$): δ = 8.20–7.35 (m, 15H; Ph), 6.10 (t, *J*(2′,3′) = *J*(3′,4′) = 10.0 Hz, 1H; H-3′), 5.94 (d, *J*(5,6) = 6.0 Hz, 1H; H-5), 5.25 (t, *J*(6,7) = *J*(7,8) = 9.5 Hz, 1H; H-7), 5.24 (d, *J*(1′,2′) = 3.5 Hz, 1H; H-1′), 5.13 (dd, *J*(1′,2′) = 3.5 Hz, *J*(2′,3′) = 10.0 Hz, 1H; H-2′), 4.87 (t, *J*(7,8) = *J*(8,8a) = 9.5 Hz, 1H; H-8), 4.83 (dd, *J*(5,6) = 6.0 Hz, *J*(6,7) = 9.5 Hz, 1H; H-6), 4.72 (d, *J*(5,6′) = 3.0 Hz, 2H; H-6′), 4.35 (t, *J*(1a,1b) = *J*(1a,8a) = 8.5 Hz, 1H; H-1a), 4.22–4.10 (m, 3H; H-1b, H-5′, H-8a), 3.49 (t, *J*(3′,4′) = *J*(4′,5′) = 10.0 Hz, 1H; H-4′), 3.47 (s, 3H; OMe), 2.06–1.80 ppm (3 s, 9H; *Me*CO); ^{13}C NMR (125.7 MHz, $CDCl_3$): δ = 169.9–165.6 (CO), 155.4 (CO), 133.6–128.4 (Ph), 97.1 (C-1′), 73.3 (C-2′), 72.5 (C-3′), 72.0 (C-8), 69.3 (C-7), 68.9 (C-6), 68.0 (C-5′), 66.0 (C-1), 63.8 (C-6′), 58.9 (C-5), 55.7 (OMe), 51.3 (C-8a), 44.5 (C-4′), 20.5–20.0 (*Me*CO); MS (ESI): *m/z*: 858.2 $[M+Na]^+$; elemental analysis calcd (%) for $C_{41}H_{41}NO_{16}S$: C 58.92, H 4.94, N 1.68, S 3.84; found: C 58.95, H 4.78, N 1.44, S 3.60.

(5*R*,6*R*,7*S*,8*R*,8a*R*)-6,7,8-Trihydroxy-5-(methyl 4-thio-α-D-glucopyranosid-4-yl)-2-oxa-3-oxoindolizidine (14): Compound **14** was obtained by conventional de-*O*-acetylation of **25** (108 mg, 0.13 mmol) with catalytic NaOMe in MeOH. Yield: 50 mg (98%); amorphous solid; R_f = 0.67 (6:3:1 MeCN/H_2O/NH_4OH); $[\alpha]_D$ = +118.7 (*c* = 1.0 in H_2O); ^{1}H NMR (500 MHz, D_2O): δ = 5.53 (d, *J*(5,6) = 6.0 Hz, 1H; H-5), 4.79 (d, *J*(1′,2′) = 4.0 Hz, 1H; H-1′), 4.60 (t, *J*(1a,1b) = *J*(1a,8a) = 9.0 Hz, 1H; H-1a), 4.34 (dd, *J*(1a,1b) = 9.0 Hz, *J*(1b,8a) = 5.5 Hz, 1H; H-1b), 4.00 (td, *J*(1a,8) = *J*(8a,8) = 9.0 Hz, *J*(1b,8a) = 5.5 Hz, 1H; H-8a), 3.93 (dd, *J*(6a′,6b′) = 12.0 Hz, *J*(5′,6a′) = 4.0 Hz, 1H; H-6a′), 3.86 (dd, *J*(5′,6b′) = 2.0 Hz, *J*(6a′,6b′) = 12.0 Hz, 1H; H-6b′), 3.81 (dd, *J*(5,6) = 6.0 Hz, *J*(6,7) = 9.5 Hz, 1H; H-6), 3.80–3.72 (m, 2H; H-3′, H-5′), 3.56 (t, *J*(6,7) = *J*(7,8) = 9.5 Hz, 1H; H-7), 3.50 (dd, *J*(1′,2′) = 4.0 Hz, *J*(2′,3′) = 10.0 Hz, 1H; H-2′), 3.49 (t, *J*(7,8) = *J*(8a,8) = 9.5 Hz, 1H; H-8), 3.34 (s, 3H; OMe), 2.77 ppm (t, *J*(3′,4′) = *J*(4′,5′) = 11.0 Hz, 1H; H-4′); ^{13}C NMR (125.7 MHz, D_2O): δ = 157.6 (CO), 99.4 (C-1′), 73.3 (C-8), 73.2 (C-3′), 73.1 (C-7), 72.2 (C-2′), 70.4 (C-6), 70.3 (C-5′), 67.1 (C-1), 61.6 (C-5), 61.1 (C-6′), 55.0 (OMe), 53.2 (C-8a), 46.0 (C-4′); MS (ESI): *m/z*: 420.1 $[M+Na]^+$; elemental analysis calcd (%) for $C_{14}H_{23}NO_{10}S$: C 42.31, H 5.83, N 3.52, S 8.07; found: C 41.99, H 5.57, N 3.21, S 7.73.

(5*S*,6*S*,7*S*,8*R*,8a*R*)-6,7,8-Trihydroxy-5-(methyl 6-amino-6-deoxy-α-D-glucopyranosid-6-yl)-2-oxa-3-oxoindolizidine (12): A solution of **26** (151 mg, 0.74 mmol) and **27** (143 mg, 0.74 mmol) in MeOH (1 mL) was stirred at 65 °C for 4 h under N_2. The solvent was eliminated under reduced pressure and the resulting residue was purified by flash chromatography (7:1 MeCN/H_2O). Yield: 89 mg (59%); syrup; R_f = 0.31 (5:1 MeCN/H_2O); $[\alpha]_D$ = +112.5 (*c* = 1.0 in H_2O); ^{1}H NMR (500 MHz, D_2O): δ = 4.74 (d, *J*(1′,2′) = 4.0 Hz, 1H; H-1′), 4.67 (d, *J*(5,6) = 3.5 Hz, 1H; H-5), 4.54 (t, *J*(1a,1b) = *J*(1a,8a) = 9.0 Hz, 1H; H-1a), 4.32 (dd, *J*(1a,1b) = 9.0 Hz, *J*(1b,8a) = 5.0 Hz, 1H; H-1b), 3.88 (ddd, *J*(1a,8) = 9.0 Hz, *J*(8a,8) = 9.7 Hz, *J*(1b,8a) = 5.0 Hz, 1H; H-8a), 3.71 (ddd, *J*(4′,5′) = 9.5 Hz, *J*(5′,6b′) = 8.0 Hz, *J*(5′,6a′) = 3.0 Hz, 1H; H-5′), 3.66–3.62 (m, 2H; H-6, H-7), 3.59 (t, *J*(2′,3′) = *J*(3′,4′) = 9.5 Hz, 1H; H-3′), 3.51 (dd, *J*(1′,2′) = 4.0 Hz, *J*(2′,3′) = 9.5 Hz, 1H; H-2′), 3.45 (m, 1H; H-8), 3.39 (s, 3H; OMe), 3.27 (t, *J*(3′,4′) = *J*(4′,5′) = 9.5 Hz, 1H; H-4′), 2.93 (dd, *J*(5′,6a′) = 3.0 Hz, *J*(6a′,6b′) = 13.5 Hz, 1H; H-6a′), 2.70 ppm (dd, *J*(5′,6b′) = 8.0 Hz, *J*(6a′,6b′) = 13.5 Hz, 1H; H-6b′); ^{13}C NMR (125.7 MHz, D_2O): δ = 158.8 (CO), 99.4 (C-1′), 73.6 (C-8), 73.0 (C-3′), 72.5 (C-7), 71.7 (C-4′), 71.3 (C-2′), 70.2 (C-6), 68.9 (C-5′), 67.1 (C-1), 66.8 (C-5), 55.3 (OMe), 52.9 (C-8a), 45.8 ppm (C-6′); MS (ESI): *m/z*: 403.1 $[M+Na]^+$; elemental analysis calcd (%) for $C_{14}H_{24}N_2O_{10}$: C 44.21, H 6.36, N 7.37; found: C 44.01, H 6.30, N 7.12.

(5*S*,6*S*,7*S*,8*R*,8a*R*)-6,7,8-Trihydroxy-5-(methyl 4-amino-4-deoxy-α-D-glucopyranosid-4-yl)-2-oxa-3-oxoindolizidine (15): A solution of **26** (70 mg, 0.34 mmol) and **28** (132 mg, 0.68 mmol, 2.0 equiv) in MeOH (1 mL) was stirred at 65 °C for 24 h under N_2 (TLC monitoring; 8:1 MeCN/H_2O). The solvent was removed under reduced pressure and the resulting residue was acetylated by treatment with Ac_2O/pyridine (1:1, 2 mL) at RT for 3 h, then subjected to flash chromatography (3:1 EtOAc/petroleum ether). Conventional deacetylation of the peracetylated residue with catalytic NaOMe in MeOH afforded **15**. Yield: 64 mg (52%); amorphous solid; R_f = 0.27 (6:1 MeCN/H_2O); $[\alpha]_D$ = −21.3 (*c* = 0.5 in H_2O). ^{1}H NMR (500 MHz, D_2O): δ = 5.08 (d, *J*(5,6) = 5.0 Hz, 1H; H-5), 4.51 (t, *J*(1a,1b) = *J*(1a,8a) = 9.0 Hz, 1H; H-1a), 4.30 (dd, *J*(1a,1b) = 9.0 Hz, *J*(1b,8a) = 5.0 Hz, 1H; H-1b), 3.87–3.81 (m, 1H; H-8a), 3.80–3.71 (m, 2H; H-6′), 3.68 (t, *J*(2′,3′) = *J*(3′,4) = 10.0 Hz, 1H; H-3′), 3.64–3.54 (m, 3H; H-6, H-7, H-5′), 3.48 (dd, *J*(1′,2′) = 4.0 Hz, *J*(2′,3′) = 10.0 Hz, 1H; H-2′), 3.41 (t, *J*(7,8) = *J*(8,8a) = 9.5 Hz, 1H; H-8), 3.32 (s, 3H; OMe), 2.57 ppm (t, *J*(3′,4′) = *J*(4′,5′) = 10.0 Hz, 1H; H-4′); ^{13}C NMR (125.7 MHz, D_2O): δ = 158.5 (CO), 99.3 (C-1′), 74.7 (C-3′), 73.4 (C-8), 72.0 (C-2′), 72.2–70.5 (C-5′, C-6, C-7), 67.3 (C-5), 66.9 (C-1), 61.0 (C-6′), 55.9 (C-4′), 54.9 (OMe), 53.2 ppm (C-8a); MS (ESI): *m/z*: 403.1 $[M+Na]^+$; elemental analysis calcd for $C_{14}H_{24}N_2O_{10}$ (380.1) C 44.21, H 6.36, N 7.37; found: C 43.94, H 6.09, N 7.18.

Glycosidase inhibition assays: Inhibitory potencies were determined spectrophotometrically by measuring the residual hydrolytic activities of

the glycosidases against the respective *o*- (for β-glucosidase/β-galactosidase from bovine liver and β-galactosidase from *E. coli*) or *p*-nitrophenyl α- or β-D-glycopyranoside, or α,α′-trehalose (for trehalase), in the presence of the corresponding glycomimetic derivative. Each assay was performed in phosphate buffer at the optimal pH for each enzyme. The K_m values for the different glycosidases used in the tests and the corresponding working pH values are listed herein: α-glucosidase (yeast): K_m = 0.35 mM (pH 6.8); isomaltase (yeast): K_m = 1.0 mM (pH 6.8); β-glucosidase (almonds): K_m = 3.5 mM (pH 7.3); β-glucosidase/β-galactosidase (bovine liver): K_m = 2.0 mM (pH 7.3); β-galactosidase (*E. coli*): K_m = 0.12 mM (pH 7.3); α-galactosidase (coffee beans): K_m = 2.0 mM (pH 6.8); trehalase (pig kidney): K_m = 4.0 mM (pH 6.2); amyloglucosidase (*Aspergillus niger*): K_m = 3.0 mM (pH 5.5); β-mannosidase (*Helix pomatia*): K_m = 0.6 mM (pH 5.5); α-mannosidase (jack bean): K_m = 2.0 mM (pH 5.5); naringinase (*Penicillium decumbens*, β-glucosidase/β-rhamnosidase activity): K_m = 0.6 mM (pH 6.8). The reactions were initiated by addition of enzyme to a solution of the substrate in the absence or presence of various concentrations of inhibitor. After the mixture was incubated for 10–30 min at 37 or 55 °C, the reaction was quenched by addition of either 1 M Na_2CO_3 or a solution of Glc-Trinder (Sigma, for trehalase). The absorbance of the resulting mixture was determined at 405 or 492 nm. The K_i value and enzyme inhibition mode were determined from the slope of the Lineweaver–Burk plots and double reciprocal analysis.

NMR spectroscopy: For the structural analysis, NMR spectra were recorded at 25–35 °C, for **10**, **11**, **12**, **13**, **14** and **15**, in D_2O with a Bruker DRX 500 MHz NMR spectrometer. The highest temperature (35 °C) was necessary for NOE experiments of **10**, **11** and **12**, to bring their hydrodynamics behavior towards the extreme narrowing limit, to try to enhance the NOEs. For sample preparation, all the compounds were lyophilized twice with 99% D_2O and once finally with 99.99% D_2O (Sigma–Aldrich). Final concentrations were approximately 1 mM in 600 μL volumes. For ^{1}H NMR titration experiments on **12**, the pH in the NMR tube was varied from 7.0 to 12.5, and 1% of acetone was used to reference the chemical shifts. Selective 1D NOESY experiments were carried out by using the double pulse field gradient echo sequence with different mixing times varying from 0.2 to 2.0 s. 2D NOESY experiments were performed with several mixing times between 0.2 and 1.0 s. Interproton distances were obtained from selective experiments, increasing the linearity of NOE growth curves by normalization (PANIC methodology[46]), calculating the initial slopes by linear regression, and applying the isolated spin pair approach (ISPA) using the rigid H5–H6 distance as a reference.

Computational methods: Calculations were performed by using MacroModel 9.8 and the OPLS-2005 force field. Bulk water solvation was simulated by using the generalized Born GB/SA continuum solvent model, which treats the solvent as a fully equilibrated analytical continuum starting near the van der Waals surface of the solute.[47] A dielectric constant of 1 was used for each molecule, the sets of charges were from the force field, and extended cutoffs of 8.0, 20.0, and 4.0 Å for the van der Waals, electrostatics, and H-bond terms were used, respectively. For each molecule, 12 initial conformers were constructed (three possible conformers around ω torsion, O6-C6-C5-O5, that is, the conformers tg, gt and gg; and four "canonical" distributions of the hydroxyl hydrogen atoms, combining "clockwise" or "reverse clockwise" orientations: *cc*, *cr*, *rc*, or *rr*). Then, a systematic torsion-driven conformational search was carried out on torsions ϕ (H5-C5-O4′-C4′-H4′) and ψ (C5-O4′-C4′-H4′), covering from −180° to +180° in 20° increments. Conjugated gradients methodology was used for energy minimization with a maximum of 1000 iterations or a threshold for gradient convergence of 0.01 kJ mol^{-1} Å^{-1}. From these 12 relaxed maps, each adiabatic map was constructed by collecting the lowest energy conformer for each grid point. Each minimum from the adiabatic maps was subjected to a Monte Carlo conformational search (torsional sampling MCMM), and the resulting structures within 20 kJ mol^{-1} from the absolute minimum were saved. From this set, all molecules within 3 kcal mol^{-1} from the minimum were subjected to a multiple minimization and the results were clustered by comparing heavy atoms with a cutoff of 0.5 A. The global minimum was then subjected to stochastic dynamics simulations MC/SD at 298 K, 1.5 fs time step for integration, and a total length of 2.5 ns, with an SD-to-MC ratio of 1. From this dynamic simulation, 5000 structures were saved and analyzed for interprotonic distances. On this set, a further multiple minimization step was carried out, the results were clustered by comparing heavy atoms with a cutoff of 0.5 A, 100 structures were saved within an energy window of 20 kJ mol^{-1}, and interprotonic distances were also analyzed.

Acknowledgements

The Spanish Ministerio de Ciencia e Innovación (contract numbers CTQ2006–15515-CO2–01, CTQ2009–14551-C02–01, SAF2010–15670 and CTQ2010–15848), the Fondo Europeo de Desarrollo Regional (FEDER), the Fondo Social Europeo (FSE), and the Fundación Ramón Areces and the Junta de Andalucía, are thanked for funding. We also thank the CITIUS (Universidad de Sevilla) for technical support. J. A. acknowledges financial support from the Spanish Ministerio de Ciencia e Innovación through the Ramon y Cajal program.

[1] a) K. M. Robinson, M. E. Begovic, B. L. Rhinehart, E. W. Heineke, J.-B. Ducep, P. R. Kastner, F. N. Marshall, C. Danzin, *Diabetes* **1991**, *40*, 825–830; b) A. J. Krentz, C. J. Bailey, *Drugs* **2005**, *65*, 385–411.

[2] a) J. Q. Fan, *Biol. Chem.* **2008**, *389*, 1–11; b) T. D. Butters, *Expert Opin. Pharmacother.* **2007**, *8*, 427–435; c) Z. Yu, A. R. Sawkar, L. J. Whalen, C. H. Wong, J. W. Kelly, *J. Med. Chem.* **2007**, *50*, 94–100; d) J. Matsuda, O. Suzuki, A. Oshima, Y. Yamamoto, A. Noguchi, K. Takimoto, M. Itoh, Y. Matsuzaki, Y. Yasuda, S. Ogawa, Y. Sakata, E. Nanba, K. Higaki, Y. Ogawa, L. Tominaga, K. Ohno, H. Iwasaki, H. Watanabe, R. O. Brady, Y. Suzuki, *Proc. Natl. Acad. Sci. USA* **2003**, *100*, 15912–15917; e) T. D. Butters, H. R. Mellor, K. Narita, R. A. Dwek, F. M. Platt, *Philos. Trans. R. Soc. London Ser. B* **2003**, *358*, 927–945; f) J. Fan, S. Ishii, N. Asano, Y. Suzuki, *Nat. Med.* **1999**, *5*, 112–115; g) J. M. Benito, J. M. García Fernández, C. Ortiz Mellet, *Expert Opin. Ther. Pat.* **2011**, *21*, 885–903.

[3] a) D. Durantel, C. Alotte, F. Zoulim, *Curr. Opin. Investig. Drugs* **2007**, *8*, 125–129; b) P. Greimel, J. Spreitz, A. E. Stütz, T. M. Wrodnigg, *Curr. Top. Med. Chem.* **2003**, *3*, 513–523.

[4] a) T. M. Wrodnigg, A. J. Steiner, B. J. Ueberbacher, *Anti-Cancer Agents Med. Chem.* **2008**, *8*, 77–85; b) Y. Nishimura *Iminosugar-based antitumoural agents. In Iminosugars: From Synthesis to Therapeutic Applications* (Eds.: P. Compain, O. R. Martin) Wiley-VCH: Weinheim, Germany, **2007**, p. 269–294.

[5] G. Horne, F. C. Wilson, J. Tinsley, D. H. Willians, R, Storer, *Drug Discov. Today* **2011**, *16*, 107–118.

[6] a) J. D. McCarter, W. Yeung, J. Chow, D. Dolphin, S. G. Withers, *J. Am. Chem. Soc.* **1997**, *119*, 5792–5797; b) W. Hakamata, M. Muroi, K. Kadokura, T. Nishio, T. Oku, A. Kimura, S. Chibac, A. Takatsuki, *Bioorg. Med. Chem. Lett.* **2005**, *15*, 1489–1492; c) C.-W. Ho, Y.-N. Lin, C.-F. Chang, S.-T. Li, Y.-T. Wu, C.-Y. Wu, C.-F. Chang, S.-W. Liu, Y.-K. Li, C.-H. Lin, *Biochemistry* **2006**, *45*, 5695–5702.

[7] a) H. Driguez, *Top. Curr. Chem.* **1997**, *187*, 85–116; b) Z. J. Witczak, J. M. Culhane, *Appl. Microbiol. Biotechnol.* **2005**, *69*, 237–244; c) W. Zou, *Curr. Top. Med. Chem.* **2005**, *5*, 1363–1391.

[8] a) J. F. Espinosa, F. J. Cañada, J. L. Asensio, M. Martín-Pastor, H. Dietrich, M. Martín-Lomas, R. R. Schmidt, J. Jiménez-Barbero, *J. Am. Chem. Soc.* **1996**, *118*, 10862–10871; b) R. Ravishankar, A. Surolia, M. Vijayan, S. Lim, Y. Kishi, *J. Am. Chem. Soc.* **1998**, *120*, 11297–11303; c) J. F. Espinosa, M. Bruix, O. Jarreton, T. Skrydstrup, J. M. Beau, J. Jiménez-Barbero, *Chem. Eur. J.* **1999**, *5*, 442–448; d) J. Jiménez-Barbero, J. F. Espinosa, J. L. Asensio, F. J. Cañada, A. Poveda, *Adv. Carbohydr. Chem. Biochem.* **2000**, *56*, 235–284.

[9] A. García-Herrero, E. Montero, J. L. Muñoz, J. F. Espinosa, A. Vián, J. L. García, J. L. Asensio, F. J. Cañada, J. Jiménez-Barbero, *J. Am. Chem. Soc.* **2002**, *124*, 4804–4810.

[10] D. A. Kuntz, C. A. Tarling, S. G. Withers, D. R. Rose, *Biochemistry* **2008**, *47*, 10058–10068.

[11] a) C. R. Johnson, A. Golebiowski, H. Sundram, M. W. Miller, R. L. Dwaihy, *Tetrahedron Lett.* **1994**, *35*, 653–654; b) H. Paulsen, K. Todt, *Adv. Carbohydr. Chem.* **1968**, *23*, 115–232.

[12] a) J. S. Andrews, T. Weimar, T. P. Frandsen, B. Svensson, B. M. Pinto, *J. Am. Chem. Soc.* **1995**, *117*, 10799–10804; b) L. M. Kavlekar, D. A. Kuntz, X. Wen, B. D. Johnston, B. Svensson, D. R. Rose, B. M. Pinto, *Tetrahedron: Asymmetry* **2005**, *16*, 1035–1046.

[13] a) I. Cumpstey, C. Ramstadius, K. E. Borbas, D. S. Alonzi, T. D. Butters, *Bioorg. Med. Chem.* **2011**, *19*, 5219–5223; b) T. K. M. Shing, H. M. Cheng, *J. Org. Chem.* **2010**, *75*, 3522–3525; c) T. K. M. Shing, H. M. Cheng, W. F. Wong, C. S. K. Kwong, J. Li, C. B. S. Lau, P. S. Leung, C. H. K. Cheng, *Org. Lett.* **2008**, *10*, 3145–3149.

[14] a) I. Cumpstey, J. Frigell, E. Pershagen, T. Akhtar, E. Moreno-Clavijo, I. Robina, D. S. Alonzi, T. Butters, *Beilstein J. Org. Chem.* **2011**, *7*, 1115–1123; b) T. Akhtar, I. Cumpstey, *Tetrahedron Lett.* **2007**, *48*, 8673–8677.

[15] a) P. Compain, *Iminosugar C-glycosides: synthesis and biological activity. In Iminosugars: From synthesis to therapeutic applications* (Eds.: P. Compain, O. R. Martin), John Wiley & Sons, Chichester, UK, **2007**, pp. 63–86; b) P. Vogel, S. Gerber-Lemaire, L. Juilleratt-Jeanneret. *Imino-C-disaccharides and analogues: synthesis and biological activity In Iminosugars: From synthesis to therapeutic applications* (Eds.: P. Compain, O. R. Martin), John Wiley & Sons, Chichester, UK, **2007**, pp. 87–130.

[16] J. L. Asensio, F. J. Cañada, A. García-Herrero, M. T. Murillo, A. Fernández-Mayoralas, B. A. Johns, J. Kozak, Z. Zhu, C. R. Johnson, J. Jiménez-Barbero, *J. Am. Chem. Soc.* **1999**, *121*, 11318–11329.

[17] For selected recent contributions on the synthesis of sp^2-iminosugars, see: a) M. Aguilar-Moncayo, P. Díaz-Pérez, J. M. García Fernández, C. Ortiz Mellet, M. I. García-Moreno, *Tetrahedron* **2012**, *68*, 681–689; b) M. Aguilar-Moncayo, M. I. García-Moreno, A. Trapero, M. Egido-Gabás, A. Llebaria, J. M. García Fernández, C. Ortiz Mellet, *Org. Biomol. Chem.* **2011**, *9*, 3698–3713; c) M. Aguilar-Moncayo, M. I. García-Moreno, A. E. Stütz, J. M. García Fernández, T. M. Wrodnigg, C. Ortiz Mellet, *Bioorg. Med. Chem.* **2010**, *18*, 7439–7445; d) M. Aguilar-Moncayo, T. M. Gloster, J. P. Turkenburg, M. I. García-Moreno, C. Ortiz Mellet, G. J. Davies J. M. García Fernández, *Org. Biomol. Chem.* **2009**, *7*, 2738–2747; e) M. Aguilar-Moncayo, M. I. García-Moreno, C. Ortiz Mellet, J. M. García Fernández, *J. Org. Chem.* **2009**, *74*, 3595–3598.

[18] For selected recent contributions on the therapeutic potential of sp^2-iminosugars, see: a) I. Silman, Y. Shaaltiel, D. Aviezer, J. L. Sussman, A. H. Futerman, C. Ortiz Mellet, *Org. Biomol. Chem.* **2011**, *9*, 4160–4167; b) Z. Luan, K. Higaki, M. Aguilar-Moncayo, L. Li, H. Ninomiya, E. Nanba, K. Ohno, M. I. Garía-Moreno, C. Ortiz Mellet, J. M. García Fernández, Y. Suzuki, *ChemBioChem* **2010**, *11*, 2453–2464; c) B. Brumshtein, M. Aguilar-Moncayo, M. I. García-Moreno, C. Ortiz Mellet, J. M. García Fernández, I. Silman, Y. Shaaltiel, D. Aviezer, J. L. Sussman, A. H. Futerman, *ChemBioChem* **2009**, *10*, 1480–1485; d) Z. Luan, K. Higaki, M. Aguilar-Moncayo, H. Ninomiya, K. Ohno, M. I. García-Moreno, C. Ortiz Mellet, J. M. García Fernández, Y. Suzuki, *ChemBioChem* **2009**, *10*, 2780–2792; e) M. Aguilar-Moncayo, T. Takai, K. Higaki, T. Mena-Barragán, Y. Hirano, K. Yura, L. Li, Y. Yu, H. Ninomiya, M. I. García Moreno, S. Ishii, Y. Sakakibara, K. Ohno, E. Nanba, C. Ortiz Mellet, J. M. García Fernández, Y. Suzuki, *Chem. Commun.*, DOI: 10.1039/c2cc32065g.

[19] E. M. Sánchez-Fernández, R Rísquez-Cuadro, M. Chasseraud, A. Ahidouch, C. Ortiz Mellet, H. Ouadid-Ahidouch, J. M. García Fernandez, *Chem. Commun.* **2010**, *46*, 5328–5330.

[20] a) P. Díaz Pérez, M. I. García-Moreno, C. Ortiz Mellet, J. M. García Fernández, *Eur. J. Org. Chem.* **2005**, 2903–2913; b) V. M. Díaz Pérez, M. I. García-Moreno, C. Ortiz Mellet, J. Fuentes, J. C. Díaz Arribas, F. J. Cañada J. M. García Fernández, *J. Org. Chem.* **2000**, *65*, 136–143; c) J. L. Jiménez Blanco, V. M. Díaz Pérez, C. Ortiz Mellet, F. Fuentes, J. M. García Fernández, J. C. Díaz Arribas, F. J. Cañada, *Chem. Commun.* **1997**, 1969–1970.

[21] B. L. Cantarel, P. M. Coutinho, C. Rancurel, T. Bernard, V. Lombard, B. Henrissat, *Nucleic Acid Res.* **2009**, *37*, D233-D238.

[22] N. A. Khan, N. R. Eaton, *Biochim. Biophys. Acta* **1967**, *146*, 173–180.

[23] R. B. Needleman, H. J. Federoff, T. R. Eccleshall, B. Buchferer, J. Marmur, *Biochemistry* **1978**, *17*, 4657–4661.

[24] E. M. Sánchez-Fernández, R. Rísquez-Cuadro, M. Aguilar-Moncayo, M. I. García-Moreno, C. Ortiz Mellet, J. M. García Fernandez, *Org. Lett.* **2009**, *11*, 3306–3309.

[25] T. Fuchss, R. R. Schmidt, *J. Carbohydr. Chem.* **2000**, *19*, 677–691.

[26] a) S. Shoda *Glycoside synthesis from glycosyl halides: glycosyl fluorides. In Handbook of chemical glycosylation: Advances in stereoselectivity and therapeutic relevance* (Ed.: A. V. Demchenko), Wiley-VCH, Weinheim, **2008**, pp. 29–58; b) J. Jünnemann, J. Thiem, C. Pedersen, *Carbohydr. Res.* **1993**, *249*, 91–94.

[27] a) D. Ellis, S. E. Norman, H. M. I. Osborn, *Tetrahedron* **2008**, *64*, 2832–2854; b) M J. Kiefel, B. Beisner, S. Bennet, I. D. Holmes, M. Itzstein, *J. Med. Chem.* **1996**, *39*, 1314–1320.

[28] K. Sato, K. Sakai, M. Kojima, S. Akai, *Tetrahedron Lett.* **2007**, *48*, 4423–4425.

[29] D. Crich, H. Li, *J. Org. Chem.* **2000**, *65*, 801–805.

[30] L. A. Reed III, L. Goodman, *Carbohydr. Res.* **1981**, *94*, 91–100.

[31] T. M. Wrodnigg, B. Eder, *Top. Curr. Chem.* **2001**, *215*, 115–152.

[32] J. M. García Fernández, C. Ortiz Mellet, J. Fuentes, *J. Org. Chem.* **1993**, *58*, 5192–5199.

[33] E. J. Reist, R. R. Spencer, D. F. Calkins, B. R. Baker, L. Goodman, *J. Org. Chem.* **1965**, *30*, 2312–2317.

[34] K. Kondo, A. Hayamitsu, E. Shitara, F. Kojima, Y. Nishimura, *Bioorg. Med. Chem. Lett.* **2001**, *11*, 1091–1095.

[35] a) S. Chandrasekhar, *ARKIVOC* **2005**, 37–66; b) V. G. Box, *J. Mol. Struct.* **2000**, *522*, 145–164.

[36] A. Imberty, S. Pérez, *Chem. Rev.* **2000**, *100*, 4567–4588.

[37] Y. Nishida, H. Hori, H. Ohrui, H. Meguro, *J. Carbohydr. Chem.* **1988**, *7*, 239–250.

[38] a) M. K. Dowd, P. J. Reilly, A. D. French, *Biopolymers* **1994**, *34*, 625–638; b) C. S. Pereira, D. Kony, R. Baron, M. Müller, W. F. van Gunsteren, P. H. Hünenberger, *Biophys. J.* **2006**, *90*, 4337–4344.

[39] A. D. French, M. K. Dowd, *J. Mol. Struct.* **1983**, *91-111*, 183–201.

[40] K. Bock, J. Ø. Duus, S. Refn, *Carbohydr. Res.* **1994**, *253*, 51–67.

[41] K. Yamamoto, H. Miyake, M. Kusunoki, S. Osaki, *FEBS J.* **2010**, *277*, 4205–4214.

[42] a) P. M. Coutinho, M. K. Dowd, P. J. Reilly, *Carbohydr. Res.* **1997**, *297*, 309–324; b) K. Bharatham, N. Bharatham, K. H. Park, K. W. Lee, *J. Mol. Graphics Modell.* **2008**, *26*, 1202–1212.

[43] T. P. Frandsen, M. M. Palcic, B. Svensson, *Eur. J. Biochem.* **2002**, *269*, 728–734.

[44] a) W. Zhong, D. A. Kuntz, B. Ember, H. Singh, K. W. Moremen, D. R. Rose, G.-J. Boons, *J. Am. Chem. Soc.* **2008**, *130*, 8975–8983.

[45] G. A. Venter, R. P. Mattews, K. Naidoo, *Mol. Simul.* **2008**, *34*, 391–401.

[46] H. Hu, K. Krishnamurthy, *J. Magn. Reson.* **2006**, *182*, 173–177.

[47] W. C. Still, A. Tempczyk, R. C. Hawley, T. Hendrickson, *J. Am. Chem. Soc.* **1990**, *112*, 6127–6129.

Received: January 25, 2012
Revised: February 28, 2012
Published online: June 4, 2012

